EBAG9 adds a new layer of control on large dense-core vesicle exocytosis via interaction with Snapin

Constantin Rüder[1], Tatiana Reimer[1], Ignacio Delgado-Martinez [2], Ricardo Hermosilla[3], Arne Engelsberg[1,5], Ralf Nehring[2], Bernd Dörken[1,4], and Armin Rehm[1,4 *]

[1] Max-Delbrück-Center for Molecular Medicine, Department of Hematology, Oncology and Tumorimmunology, Berlin, Germany
[2] Max-Planck-Institut für Biophysikalische Chemie, Abteilung Membranbiophysik; Göttingen, Germany
[3] Universitätsmedizin Berlin, Charite, Universitätsklinikum Benjamin-Franklin, Department of Pharmacology, Berlin, Germany
[4] Universitätsmedizin Berlin, Charite, Robert-Rössle-Klinik, Department of Hematology, Oncology and Tumorimmunology, Berlin, Germany

*Corresponding Author: Dr. Armin Rehm
Max-Delbrück-Center for Molecular Medicine
Department of Hematology, Oncology and Tumorimmunology
Robert-Rössle-Str. 10
13125 Berlin, Germany
Fax: (49) 30-9406 2698
Email: arehm@mdc-berlin.de

[5] Present address: Institute for Molecular Neurobiology, Freie Universität Berlin, Berlin, Germany

Running Title: Involvement of EBAG9 in exocytosis

Key Words: Tumor-associated antigen; regulated exocytosis; phosphorylation; subcellular localization; SNARE-complex

Abstract

Regulated exocytosis is subject to several modulatory steps that include phosphorylation events and transient protein-protein interactions. The EBAG9 gene product was recently identified as a modulator of tumor-associated O-linked glycan expression in non-neuronal cells, however this molecule is expressed physiologically in essentially all mammalian tissues. Particular interest gained this molecule because in some human tumor entities high expression levels correlated with clinical prognosis.

To gain insight into the cellular function of EBAG9, we scored for interaction partners employing the yeast two-hybrid system. Here, we demonstrate that EBAG9 interacts with Snapin, which is likely to be a modulator of Synaptotagmin-associated regulated exocytosis. Strengthening of this interaction inhibited regulated secretion of neuropeptide Y from PC12 cells, whereas evoked neurotransmitter release from hippocampal neurons remained unaltered. Mechanistically, EBAG9 decreased phosphorylation of Snapin, subsequently association of Snapin with SNAP25 and SNAP23 was diminished. We suggest that the occurrence of SNAP23, Snapin and EBAG9 also in non-neuronal cells might extend the modulatory role of EBAG9 to a broad range of secretory cells. The conjunction between EBAG9 and Snapin adds an additional layer of control on the exocytosis process, in addition mechanistic evidence is provided that inhibition of phosphorylation has a regulatory function in exocytosis.

Introduction

The secretion of biomolecules in many types of eukaryotic cells is mediated through both the constitutive and regulated transport of vesicles (Burgess and Kelly, 1987). Whereas constitutive exocytosis involves a continuous flow and fusion of vesicles between cellular organelles and to the plasma membrane, regulated exocytosis is characterized by vesicle trafficking, followed by vesicle fusion with the target membrane only in the presence of elevated levels of cytoplasmic Ca^{2+} (Burgoyne and Morgan, 2003). The best studied variant of regulated exocytosis includes the synaptic transmission in neuronal and neuroendocrine cells, where upon arrival of the Ca^{2+} trigger neurotransmitter release from preformed vesicles is effectuated (Chen *et al.*, 1999; Jahn and Südhof, 1999; Rettig and Neher, 2002).

Consent has emerged that vesicle fusion with a target membrane is a stepwise process that involves several protein families including SNAREs, Rab proteins and Sec1/Munc-18 related molecules (Jahn and Südhof, 1999). The synaptic vesicle cycle starts with the tethering and docking of vesicles in the active zones of the plasma membrane, followed by a priming step that includes the formation of a SNARE complex (Fernandez-Chacon and Südhof, 1999; Südhof, 1995). SNAREs are a superfamily of small and mostly membrane-anchored proteins that share a common motif of about 60 amino acids. A functional neuronal SNARE complex in cells is formed between SNARE proteins residing in vesicle membranes, including VAMP, and the plasma membrane with the t-SNARE proteins Syntaxin and SNAP25 (Söllner *et al.*, 1993; Sutton *et al.*, 1998).

The candidate Ca^{2+} sensor Synaptotagmin I is localized to synaptic vesicles and large dense-core vesicles (LDCV) (Brose *et al.*, 1992; Geppert *et al.*, 1994). Synaptotagmin I acts at a postdocking step in exocytosis, including a maturation step of primed vesicles into the readily releasable pool of vesicles (RRP) (Voets *et al.*, 2001), but also a final fusion-pore opening stage (Chapman, 2002; Wang *et al.*, 2001). Recently, a novel SNAP25 interacting protein,

Snapin, was identified. It was suggested that cAMP-dependent protein kinase (PKA) mediated phosphorylation of Snapin enhanced binding to SNAP25. This interaction improved the binding affinity of Synaptotagmin I to SNAP25 and the SNARE complex *in vitro*. Employing a phosphomimetic mutant of Snapin, an increase in size of the exocytotic burst, but also an enhanced sustained component of exocytosis in chromaffin cells was seen (Chheda *et al.*, 2001; Ilardi *et al.*, 1999). In support of a more general role in intracellular membrane fusion events, additional Snapin-interacting proteins were identified that are not limited to neuronal transmitter release, among them novel subunits of the biogenesis of lysosome-related organelles complex-1 (BLOC-1) and adenylyl cyclase VI (Chou *et al.*, 2004; Starcevic and Dell'Angelica, 2004).

In this study, we refer to our previous report on EBAG9 (*estrogen receptor-binding fragment-associated gene9*), also termed RCAS1 (*receptor-binding cancer antigen expressed on SiSo cells*), which caused the occurrence of tumor-associated O-linked glycans on cell lines that are normally negative for these antigens. EBAG9 is an estrogen-inducible, ubiquitously expressed protein with close homologues in human and murine rodents that exhibits a Golgi-predominant localization in non-neuronal cells (Engelsberg *et al.*, 2003; Tsuchiya *et al.*, 2001). This raised the question what function EBAG9 under physiological conditions has and if this function relates to its proposed tumor-association (Akahira *et al.*, 2004; Ikeda *et al.*, 2000; Kubokawa *et al.*, 2001; Leelawat *et al.*, 2003; Suzuki *et al.*, 2001; Tsuneizumi *et al.*, 2001). Using full-length EBAG9 as the bait to screen a human brain cDNA library, we identified Snapin as an interaction partner of EBAG9 and verified the relevance of this interaction in exocytosis assays. Overexpression of EBAG9 inhibited regulated secretion of neuropeptide Y (NPY) in intact PC12 cells, whereas constitutive secretion of α1-antitrypsin in HepG2 cells remained unaffected. In contrast, EBAG9 overexpression in hippocampal neurons did not alter synaptic transmission. Mechanistically, EBAG9 inhibited Snapin phosphorylation, which subsequently attenuated Snapin binding to SNAP25 and SNAP23.

These data demonstrate that EBAG9 is a novel modulator of regulated exocytosis that acts upstream of Snapin and the SNARE complex.

Materials and Methods

Cell culture and transfections

HEK293 and HepG2 cells were cultured in DMEM medium (PAA), supplemented with 10% FCS (Biochrom), 2 mM L-glutamine and 100 U/ml penicillin-streptomycin. PC12 cells were grown with additional 10% horse serum (Invitrogen). HEK293 cells were transfected by electroporation using a Biorad Gene Pulser. PC12 cells were transfected by using Lipofectamine 2000 (Invitrogen).

Antibodies

A polyclonal rabbit anti-EBAG9 serum was described previously (Engelsberg *et al.*, 2003). Monoclonal antibodies (mAb) against Synaptophysin and VAMP2 were obtained from Synaptic Systems, mAbs against EEA1, GM130 and p115 were from BD Biosciences, and anti-Flag mAbs M2 and M5 were from Sigma. Biotinylated anti-GFP antibody was purchased from Vector Laboratories, goat anti-α1-antitrypsin antibody was from US Biological and goat anti-GST antibody from Pharmacia. A rabbit anti-GFP serum was used for immunoprecipitation (a kind gift of R. Schülein, Berlin), and a rabbit anti-Snapin serum was kindly provided by R. Jahn (Göttingen) (Vites *et al.*, 2004).

Expression plasmid constructs

Deletion variants or site-directed mutants of EBAG9 (Engelsberg *et al.*, 2003) and Snapin were constructed by PCR using sequence specific primer pairs (see Supplementary Information S1). Full length Snapin cDNA was isolated in a yeast two-hybrid screen from a human brain cDNA library (kindly provided by H.-J. Schäffer, Berlin). GST-SNAP23 was generated by PCR using SNAP23-pcB7 (Koticha *et al.*, 1999) as template. All constructs were verified by cDNA sequencing.

Generation of recombinant fusion proteins, *in vitro* transcription and translation

The expression of GST and His_6-fusion proteins in E. coli DH5α was done essentially as described (Smith and Johnson, 1988). Briefly, fusion protein constructs were cloned into pGEX-4T-1 (Amersham) or pQE-32, respectively (Qiagen), followed by induction with 1 mM IPTG. Bacterial pellets were sonicated and lysed in PBS/0.5% TX-100. GST or polyhistidine-tagged fusion proteins were purified by binding to glutathione-sepharose (Amersham) beads or Ni-NTA agarose (Qiagen), respectively. Quantification of recovered fusion protein was done by Bradford protein assay and by SDS-PAGE and Coomassie Brilliant Blue staining. *In vitro* transcription and translation were performed in the presence of [^{35}S] methionine/cysteine (Express protein labeling mix, NEN), according to the manufacturers instructions using Promega Riboprobe kit (Promega) and the Promega Flexi rabbit reticulocyte system.

Yeast two-hybrid screen

A full length human EBAG9 cDNA was inserted in-frame into pGBKT7 bait vector (Clontech) containing the GAL4 DNA-binding domain (BD). Expression was confirmed by SDS-Page and immunoblotting. Yeast cells (AH109) were sequentially transformed with pGBKT7-EBAG9 bait vector and a human brain cDNA library in the GAL4 activation domain (AD) containing vector pACT2 (Clontech) according to the protocols described for the MATCHMAKER GAL4 Two-Hybrid System 3 (Clontech). Transformants were selected on plates lacking tryptophan, leucine, histidine and adenine and supplemented with 5-bromo-4-chloro-3-indolyl-α-D-galactopyranoside (Glycosynth). Prey plasmids from Ade^+, His^+, $Mel1^+$ clones were rescued and confirmed by re-transformation into fresh yeast cells with the pGBKT7-EBAG9 bait or various control baits. β-galactosidase (lacZ) activity was quantified by liquid culture assay using standard protocols. The prey plasmids were subjected to DNA sequencing and analyzed by BLAST search.

***In vitro* binding assays**

In vitro translated [^{35}S] labeled EBAG9 was incubated with 3 µg of the indicated GST fusion protein immobilized on glutathione-sepharose in NP-40 binding buffer (50 mM Tris, pH 7.4, 5 mM $MgCl_2$, 0.5% NP-40, 1 mM PMSF and 1.5 µg/ml aprotinin). After incubation for 3 h at 4°C, beads were washed extensively in binding buffer and bound protein was released by boiling in Laemmli reducing sample buffer. An aliquot of the sample was analyzed by 12.5% SDS-PAGE and bound [^{35}S] labeled EBAG9 was visualized by autoradiography. The remaining sample was separated by SDS-PAGE and stained with Coomassie Brilliant Blue to control equal load of various GST fusion proteins. Usually, this binding assay was done under saturating conditions.

In a competitive binding assay, 10 µg immobilized GST-SNAP25 or GST-mSNAP23 were incubated with a constant amount of *in vitro* translated [^{35}S] labeled Snapin and increasing amounts of [^{35}S] labeled EBAG9. Beads were washed extensively with 50 mM Tris, pH 7.4, 50 mM NaCl, 0.5% Triton X-100 (TX-100) and bound protein was analyzed by SDS-PAGE.

For pulldown assays, transiently transfected HEK293 cells were lysed in binding buffer (25 mM Hepes, pH 7.4, 140 mM KCl, 20 mM NaCl, 0.5% CHAPS). 300 µg cell lysate were incubated with 4.5 µg of the indicated GST fusion protein immobilized on glutathione-sepharose beads in binding buffer (0.3% CHAPS). Beads were washed in binding buffer, resuspended in sample buffer and separated using SDS-PAGE. Bound EBAG9-GFP was visualized with biotinylated anti-GFP antibody. For binding assays with Snapin-GFP, transfected HEK293 cells were lysed in binding buffer (50 mM Tris, pH 7.4, 50 mM NaCl, 0.5% TX-100). Cell lysates were incubated with the indicated GST fusion proteins in binding buffer containing 0.1% TX-100. Beads were processed as shown before.

Coimmunoprecipitation, gel electrophoresis and immunoblotting

Cell extracts were prepared from cotransfected HEK293 cells using TX-100 containing lysis buffer (50 mM Tris, pH 7.4, 50 mM NaCl, 0.5% TX-100). Solubilized proteins were incubated with 5 µg of anti-Flag mAb M5 or rabbit anti-GFP serum and protein A-sepharose (Amersham) in binding buffer (50 mM Tris, pH 7.4, 50 mM NaCl, 0.1% BSA, 0.1% TX-100). Beads were washed three times with binding buffer and bound proteins were separated on a 12.5% SDS-PAGE, followed by transfer to nitrocellulose membranes. Blots were further processed as described, employing primary antibodies as detailed in the Figure legends (Rehm and Ploegh, 1997).

Determination of the ratio between total recombinant Snapin-GFP and Flag-tagged EBAG9 in cell lysates in relation to their amount found in a complex with their respective binding partner was assessed by densitometric scanning of bands obtained from immunoblotting using identical antibodies. Usually, 1/40 volume of the cell lysate was used to assess total cellular content of the fusion proteins.

Laser Scanning Microscopy

HEK293 cells were cotransfected with Snapin-GFP and pcDNA-EBAG9 and grown on coated coverslips for 36 h, essentially as described (Engelsberg *et al.*, 2003). Bound antibodies were detected with a biotinylated secondary antibody (Southern Biotechnology) and Streptavidin conjugated Alexa Fluor^{TM} 568 (Molecular Probes). Confocal images were acquired with a confocal laser scanning microscope LSM510 (Zeiss). Fluorescence signals were detected using the following configurations: GFP λ_{exc} = 488 nm, BP λ_{em} = 500-530 nm and AlexaFluor568 λ_{exc} = 543 nm, LP λ_{em} = 560 nm, respectively. Acquisition was performed using a multi track to prevent bleed-through. All images were processed using LSM Examiner or LSM Browser software.

For confocal microscopic analysis of PC12 cells, cells were grown on collagen coated coverslips. Where indicated, PC12 cells were stimulated for 3 days with nerve growth factor (ß-NGF; 150 ng/ml; Sigma). Zeiss LSM510 software was used for quantification of fluorescence intensities along representative lines through intracellular regions and through neurite extensions.

Gel Filtration and Subcellular Fractionation

PC12 cells were solubilized in lysis buffer (50 mM Tris/HCl, pH 7.4, 50 mM NaCl, 1 mM $MgCl_2$, 0.5% CHAPS and protease inhibitors), and precleared cell lysate was applied to a Superdex 200 16/60 column (Amersham), preequilibrated with elution buffer (50 mM Tris/HCl, pH 7.4, 50 mM NaCl, 0.2% CHAPS) at a flow rate of 0.3 ml/min. Fractions (1.5 ml) were precipitated with TCA and analyzed by immunoblotting. For the assessment of void volume (V_0) the column was calibrated with blue dextran (2000 kD) and for the determination of molecular weight the protein standards ferritin (440 kD), aldolase (158 kD), ovalbumin (43 kD) and ribonuclease A (14 kD) were used.

For subcellular fractionation experiments, PC12 cells were stimulated for 3 d with ß-NGF (150 ng/ml), and cell homogenization and fractionation on a discontinuous sucrose gradient was performed exactly as described (Rehm and Ploegh, 1997). Briefly, a postnuclear supernatant was adjusted to 40% (w/v) sucrose in a buffer containing 10 mM Tris/HCl, pH 7.4, and layered on a 50% sucrose solution. Subsequently, a discontinuous sucrose gradient consisting of 35, 25, 15 and 0% (w/v) was poured on top of the 40% sucrose fraction. The gradient was centrifuged for 16 h at 170,000 xg (SW41 rotor). Fractions were harvested (0.75 ml) from the top and analyzed by immunoblotting.

Generation of adenovirus vectors and transduction of cell lines

EBAG9 was subcloned in the expression cassette of pQBI-AdCMV5-GFP (Q-Biogene), followed by homologous recombination with a viral backbone vector in HEK293A cells. Ad-EBAG9-GFP and Ad-GFP were expanded, purified and titered as described (Cichon *et al.*, 1999).

Generation of Semliki Forest Virus

Wild-type EBAG9 was cloned into the Semliki Forest Virus expression vector (based on pSFV1; Invitrogen) containing the respective EBAG9 cDNA sequence fused to EGFP (Ashery *et al.*, 1999).

NPY release assay

NPY-T7-GST secretion assay in PC12 cells was essentially performed as described previously (Fukuda, 2003). Briefly, PC12 cells (6-cm dish) were cotransfected with pShooter-NPY-T7-GST and EBAG9-GFP, EBAG9-GFP C12/14/27S or GFP (mock). Three days after transfection, cells were stimulated with either high KCl buffer (56 mM KCl, 95 mM NaCl, 2.2 mM $CaCl_2$, 0.5 mM $MgCl_2$, 5.6 mM glucose, and 15 mM Hepes, pH 7.4) or low KCl buffer (5.6 mM KCl, 145 mM NaCl, 2.2 mM $CaCl_2$, 5.6 mM glucose, 0.5 mM $MgCl_2$, and 15 mM HEPES, pH 7.4) for 10 min at 37 °C. Released NPY-T7-GST was recovered by incubation with glutathione-sepharose beads. After extensively washing with NP-40 lysis buffer (0.5% NP-40, 50 mM Tris, pH 7.4, 5 mM $MgCl_2$) proteins bound to the beads were analyzed by 12.5 % SDS-PAGE followed by immunoblotting with anti-GST antibody. The intensity of the immunoreactive bands on x-ray film was quantified by computer analysis (Tina 2.0, Raytest).

Metabolic Labeling and α1-antitrypsin secretion

HepG2 cells were infected with Ad-EBAG9-GFP or Ad-GFP at the MOI indicated in the Figure legend. Cells were starved, metabolically labeled with 250 μCi of [^{35}S] methionine/cysteine for 10 min and chased essentially as described (Rehm and Ploegh, 1997). After the chase, cells were washed in PBS and lysed in NP-40 buffer (see above). α1-antitrypsin was immunoprecipitated from precleared cell lysates and from culture supernatant with anti-α1-antitrypsin antibody immobilized on protein A-sepharose. Bound protein was analyzed by SDS-PAGE and autoradiography. Protein levels were quantified by densitometric scanning.

For palmitoylation, HEK293 cells were transiently transfected with EBAG9-GFP, GFP or EBAG9-mutants. 24 h after transfection, cells were incubated in serum-free medium for 16 h, followed by labeling with [^{3}H] palmitic acid (400 μCi/ml) for 4 h. GFP or GFP-tagged proteins were recovered from NP-40 lysates with anti-GFP serum. Immunoprecipitates were analyzed on SDS-PAGE under non-reducing conditions. Gels were fixed with 10% methanol/10% acetic acid for 90 min before autoradiography. In some experiments, [^{3}H]palmitate labeled immunoprecipitates were split and aliquots were run on separate lanes on SDS-PAGE. After fixation, gels were cut and identical immunoprecipitates were subjected to either 1 M Tris/HCl (pH 7.4) or 1 M hydroxylamine/HCl (pH 7.4) treatment before autoradiography.

Phosphorylation Experiments

Snapin-GFP was cotransfected with an equal amount of pcDNA-EBAG9 or empty vector (mock). Cells were starved for 1 h in phosphate-free DMEM (ICN), followed by metabolic labeling with 500 μCi [^{32}P] orthophosphoric acid (ICN) for 1 h in phosphate-free DMEM. Cells were then stimulated with PMA (30 ng/ml), Forskolin (40 μM), or remained

unstimulated for 10 min at 37°C. Phosphorylated cells were washed and lysed in RIPA buffer (50 mM Tris, pH 7.5, 50 mM NaCl, 0.5% NP-40, 0.25% deoxycholate, 0.5 mM EDTA, 1 mM Na_3VO_4, 10 mM NaF and protease inhibitors) for 1 h at 4°C. Snapin was immunoprecipitated with rabbit anti-GFP serum, immunoprecipitates were resolved by SDS-PAGE and Snapin was visualized by autoradiography. Snapin phosphorylation levels were quantified and normalized for Snapin protein loads, as assessed by immunoblotting. *In vitro* phosphorylation experiments were performed essentially as described previously (Chheda *et al.*, 2001), using 1 U/µl catalytic subunit PKA (Promega) or casein kinase II (CKII) (NEB). Phosphorylation levels were quantified by phosphorscreen and normalized to equimolar protein amounts, as determined by Coomassie Brilliant Blue staining.

Electrophysiological analysis of cultured hippocampal neurons

Microisland cultures of mouse hippocampal neurons were prepared from NMRI mice and maintained as described (Reim *et al.*, 2001). Neurons were grown in a chemically defined medium (NBA+B27, GibcoBRL) and infected with Semliki Forest Virus after 10-14 d *in vitro*. For each experiment, approximately equal numbers of infected and uninfected control cells from the same preparation were measured in parallel and blindly 8-10 h after infection. Recording conditions (21°C), data acquisition and analysis were performed as described (Reim *et al.*, 2001; Rosenmund and Stevens, 1996).

Results

EBAG9 recruits the SNARE-associated protein Snapin

To assess the physiological role of the EBAG9 encoded gene product, we scored for intracellular interaction partners using a yeast two-hybrid screen. Full-length human EBAG9 was used as a bait for screening of a human brain cDNA library. Approximately 10^6 independent clones were screened for activation of the reporter genes Ade, His and Mel1/lacZ and 9 interacting clones were readily obtained. Strongest induction of the β-galactosidase reporter was observed for two clones, both contained full-length cDNAs encoding Snapin (Figure 1A). Specificity of the EBAG9-Snapin association was shown by transformations of control bait and prey plasmids (Figure 1B).

To confirm a selective interaction between EBAG9 and Snapin, *in vitro* binding assays using recombinant fusion proteins were performed. Since GST-EBAG9 is synthesized at extremely low rate in bacteria and is not soluble in aqueous solutions (Engelsberg *et al.*, 2003), EBAG9 was translated *in vitro* and incubated with GST-Snapin. Whereas [^{35}S] labeled EBAG9 associated with GST-Snapin exclusively, the GST-tagged SNARE-proteins SNAP25, VAMP2 and GST alone failed to recover EBAG9 in this *in vitro* pulldown assay (Figure 2A). *In vitro* translated MHC class I heavy chain HLA-A3 failed to interact with GST-Snapin, which argued against a non-specific adsorption of Snapin (Supplementary Information S2).

EBAG9 binds to Snapin *in vivo*

The interaction between EBAG9 and Snapin was further confirmed by association of *in vitro* translated EBAG9 with GST-Snapin and by coimmunoprecipitation assays from transfected HEK293 cells. Although various epitope-tagged Snapin eukaryotic expression plasmids were generated, only a polyclonal anti-GFP antibody was suitable to immunoprecipitate GFP-

tagged Snapin. A specific binding of properly folded Snapin to the GST-fusion proteins SNAP25 and SNAP23 was revealed (Figure 2B). The ubiquitously expressed SNAP25 homologue, SNAP29, failed to interact with Snapin-GFP.

Coimmunoprecipitation of Snapin-GFP and N-Flag-EBAG9 in cotransfected HEK293 cells was seen employing the anti-Flag antibody M5 (Figure 2C). Reciprocal coimmunoprecipitation yielded the same results (Figure 2D). Bound Snapin accounted for 4% of recombinant Snapin expressed in the starting material, as determined by densitometric scanning of bands obtained in total lysate and following coimmunoprecipitation. Conversely, the determination of recombinant Flag-tagged EBAG9 associated with Snapin yielded in an amount of approximately 12% related to the total cell lysate. These rates could reflect transient interactions and relate to the number of fully assembled SNARE complexes in neuronal cells, which is in the range of 4-5% (Matveeva *et al.*, 2003).

To further support our observation that EBAG9 and Snapin proteins are associated *in vivo*, we subjected a PC12 cell extract to size exclusion chromatography on a Sephadex 200 column. The majority of both EBAG9 and Snapin eluted at a molecular weight larger than 440 kD with a significant cofractionation in fractions 9-15 (Figure 2E). This fractionation profile of Snapin is consistent with a recent publication showing the cofractionation of Snapin with the lysosome-related organelle complex-1 (BLOC-1) in fractions corresponding to 600 kD (Starcevic and Dell'Angelica, 2004). Only a minor proportion of Snapin (fraction 43) and EBAG9 (fractions 33-35) eluted at positions corresponding to the expected monomers. In addition, we observed the occurrence of Snapin also in fractions 27-29 (molecular weight range 66-98 kD) where EBAG9 was essentially absent. This points to the potential presence of other association partners, alternatively multimeric Snapin complexes might occur.

Identification of the binding domains relevant for EBAG9-Snapin association

To map the binding regions relevant for EBAG9-Snapin interaction, binding assays of EBAG9-GFP with GST-Snapin or truncated fusion proteins were performed. Analysis of the human Snapin-cDNA sequence applying the Coils program algorithm (Lupas *et al.*, 1991) predicted two helical regions (H1; aa37-65 and H2; aa83-126). The C-terminal coiled-coil domain (H2) was characterized as a binding domain for SNAP25 and SNAP23 (Buxton *et al.*, 2003; Ilardi *et al.*, 1999). In contrast, the N-terminal hydrophobic domain (HD; aa1-20) was suggested to be involved in membrane association of Snapin (Ilardi *et al.*, 1999). Two GST-Snapin deletion mutants, Δ1-20 and Δ83-136, were analyzed for their binding to full length EBAG9-GFP. The predicted N-terminal α-helix domain (H1) of Snapin was sufficient to confer binding to EBAG9, whereas a deletion of the predicted hydrophobic domain (Δ1-20) or the deletion of the C-terminal coiled-coil domain (Δ83-136) were dispensable for the observed association (Figure 3A). This observation argued against an unspecific interaction due to clustered basic residues in the C-terminus of Snapin.

To define the region of EBAG9 involved in binding Snapin, binding analysis of EBAG9-GFP wildtype (wt) and truncated fusion proteins with GST-Snapin were performed. Full length EBAG9 and all other mutants exhibited similar binding efficiency, whereas the N-terminal truncated variant, EBAG9-GFP Δ1-27, with a deletion of the putative TM- and intraluminal extreme N-terminus, was essentially negative. A deletion mutant that exhibited the predicted transmembrane and intraluminal short N-terminus only, EBAG9-GFP Δ30-213, was sufficient to confer binding to a GST-Snapin fragment containing the first coiled-coil domain (aa 21-82) (Figure 3B).

These data suggested that the association between EBAG9 and Snapin was mediated by the N-terminal domain of EBAG9 and the N-terminal coiled-coil domain (H1) of Snapin.

Membrane association and posttranslational modifications of EBAG9 and Snapin

Our previous study did not rule out the possibility that the predicted TM-domain (aa 8-27), which contains three cysteine residues, was palmitoylated and thus provides a lipid anchor for a peripheral membrane association of EBAG9 (Engelsberg *et al.*, 2003). To revisit this observation, the subcellular localization of the EBAG9 cysteine mutant C12/14/27S was analyzed. The mutant exhibited a dispersed cytoplasmic staining pattern, in contrast EBAG9 wt localized to the Golgi-region (Figure 4A). Palmitoylation of EBAG9 was assessed in [^{3}H] palmitic acid labeled and transiently transfected HEK293 cells. EBAG9 was immunoprecipitated from detergent lysates, and a specific band for wt EBAG9, but not for the cysteine mutant or the truncated mutant (Δ1-27) lacking the palmitoylation acceptor sites on SDS-PAGE was obtained (Figure 4B). As expected for a thioester linkage, the palmitate label was removed by treatment with neutral hydroxylamine (Figure 4C). The cytoplasmic staining pattern of the mutant implies that the subcellular localization of EBAG9 is dependent on the palmitoylation anchor, which would allow greater accessibility for the interaction with Snapin.

To explore membrane association and co- or posttranslational modifications, Snapin was translated *in vitro* in reticulocyte lysate. The cotranslational addition of microsomes did not result in a size shift in SDS-PAGE (Figure 5A). Therefore, a potential N-glycosylation site (N110) was not employed. To probe for a posttranslational membrane association of Snapin, *in vitro* translation of Snapin was stopped by the inclusion of cycloheximide and microsomes were added. Microsomal membrane bound Snapin was analyzed by SDS-PAGE, demonstrating a posttranslational association of Snapin, possibly recruited through protein-protein interactions (Figure 5B).

Snapin localizes to the cytosol of non-neuronal cells, but it was also found on perinuclear membranes and at the plasma membrane itself (Buxton *et al.*, 2003). When HEK293 cells were cotransfected with Snapin-GFP and pcDNA-EBAG9, Snapin was found in the cytosol

(green), but perinuclear staining was obtained as well (Figure 5C). In this region, signals for EBAG9 and Snapin were overlapping (merge: yellow), indicating an association of both molecules at the Golgi complex.

Subcellular localization of EBAG9 in neuroendocrine cells

Snapin is a SNARE associated protein involved in regulated secretion, therefore we explored the intracellular distribution of EBAG9 in PC12 cells which are equipped with an abundant regulated exocytosis machinery. In undifferentiated PC12 (–NGF) cells, EBAG9-GFP was predominantly localized to the perinuclear region (Figure 6A). In contrast, in NGF-stimulated PC12 cells (+NGF) EBAG9-GFP revealed an additional punctate staining pattern, with enrichments in the neurite extensions and at the cell periphery.

Neurite extensions in PC12 cells are enriched for LDCV and synaptic-like vesicles (Chilcote *et al.*, 1995). The identity of EBAG9-positive vesicular structures in NGF-stimulated PC12 cells was explored by double immunofluorescence staining with the secretory vesicle marker molecules Synaptophysin (Figure 6A) and VAMP2 (Figure 6B). Comparison of EBAG9-GFP with Synaptophysin or VAMP2 revealed a significant overlap in neurite extensions of differentiated PC12 cells (+NGF) (merge: yellow), whereas in undifferentiated cells (–NGF) the staining pattern is clearly separate (shown for Synaptophysin). Analysis of fluorescence intensities along a line in two representative areas showed a high degree of overlap, indicating sites with high concentrations of EBAG9 and VAMP2 (Figure 6C).

To score for colocalization with organelle specific markers in NGF-treated PC12 cells, a subcellular fractionation was performed (Figure 7A and B). Postnuclear supernatant prepared from PC12 cells was fractionated by equilibrium centrifugation on a discontinuous sucrose gradient. Gradient fractions were analyzed for marker proteins by immunoblotting.

We observed significant overlap of EBAG9 with the secretory vesicle marker proteins VAMP2 and Synaptophysin in the lower buoyant density region of the gradient, but also a significant cofractionation with the Golgi marker proteins p115 and GM130.

We conclude that EBAG9 is subject to a dynamic redistribution in differentiated neuroendocrine cells, as supported by a flexible lipid membrane anchor (see before).

EBAG9 inhibits regulated exocytosis

Subcellular localization in NGF-stimulated PC12 cells and association with the SNARE-associated molecule Snapin suggested a modulatory role for EBAG9 in regulated exocytosis. Employing an established neurosecretion assay in transiently transfected PC12 cells, transient overexpression of EBAG9 resulted in a statistically significant decrease (mean 46%, $p = 0.00025$) in high K^+-induced NPY-GST release (Figure 8A, left), but it had no effect on low K^+-dependent secretion (Figure 8A, right). The cysteine-deficient mutant of EBAG9 (EBAG9 C/S, also referred to as C12/14/27S) failed to inhibit NPY-secretion, indicating that only a membrane-bound form of the molecule is active in regulated exocytosis. In addition, the coexpression of Snapin was able to rescue the inhibition of evoked Norepinephrine release from intact PC12 cells upon EBAG9 overexpression (Supplementary Information S3), suggesting that EBAG9 specifically targets Snapin. This observation indicated that EBAG9 controls regulated LDCV exocytosis.

Since EBAG9 and its interaction partner Snapin are expressed ubiquitously also in non-neuronal cells, we also addressed the influence of EBAG9 on constitutive exocytosis. When HepG2 cells were infected with adenovirus encoding EBAG9 or with a control virus, no differences in absolute amounts or in the kinetics of α1-antitrypsin secretion were seen (Figure 8B). To further exclude an unspecific effect of EBAG9 overexpression on the secretory pathway, we explored the effects of EBAG9 on the ER-Golgi transport of MHC class I molecules and on the trafficking of cathepsin D from the Golgi complex to the

lysosomal compartment (Supplementary Information S4 and S5). In conclusion, we observed no difference in maturation kinetics of MHC class I molecules or cathepsin D.

Overexpression of EBAG9 does not alter neurotransmitter release in hippocampal neurons

The characteristics of synaptic transmission can be reliably studied in primary cultures. The culture system of choice is the autaptic microdot culture in which individual neurons are plated on small astrocyte feeder islands and generate recurrent or autaptic synapses with themselves. This culture system has been used successfully in the analysis of a number of mouse deletion mutants lacking essential presynaptic proteins, e.g. Synaptotagmin I and Complexin (Geppert *et al.*, 1994; Reim *et al.*, 2001).

Standard patch clamp recordings from single isolated neurons were used to assess possible defects of presynaptic properties using a Semliki Forest Virus construct (Ashery *et al.*, 1999) encoding for EBAG9-GFP. Synaptic responses were evoked by brief somatic depolarisation (2 ms depolarisation from -70 mV holding potential to 0 mV) 8-10 h postinfection and measured as peak inward currents a few ms after action potential induction (Figure 9A). We concentrated our analysis on excitatory glutamatergic neurons, as they are much more abundant than inhibitory GABAergic cells in autaptic cultures. EPSC amplitudes recorded from neurons overexpressing EBAG9 were similar to eGFP expressing cells (3.0 ± 0.37 nA for control and 3.40 ± 0.65 nA for EBAG9 overexpressing neurons; $p = 0.52$)

Sizes of RRP were quantified by measuring the responses of mutant cells and their appropriate controls to application of 500 mM hypertonic sucrose solution for 4 s. Typically, this treatment induces release of the RRP, which in turn leads to a transient inward current followed by a steady current component (Rosenmund and Stevens, 1996) (Figure 9B). The transient part consists of a burst-like release of vesicles resulting from the forced fusion of all

fusion competent, primed vesicles. The total number of vesicles in the RRP of a cell can therefore be quantified by integrating the total charge of the transient current component after application of hypertonic solution, divided by the charge of the average mEPSC. As shown in Figure 8B, the postsynaptic currents measured during application of hypertonic sucrose were not significantly different between control cells (0.56 ± 0.25 nC) and EBAG9 overexpressing neurons (0.49 ± 0.08 nC; p = 0.36).

When tested at higher stimulation rates, EPSCs from EBAG9 overexpressing cells and control cells showed similar degrees of depression (Figure 9C). We conclude that the effects seen for the EBAG9-Snapin interaction depend on the regulated exocytosis system, as explored in hippocampal neurons or in PC12 cells, respectively.

EBAG9 inhibits the basal phosphorylation of Snapin

Snapin has been suggested to be a substrate for the cAMP-dependent protein kinase A (PKA), leading to enhanced association with SNAP25 and increased exocytosis (Chheda *et al.*, 2001). Based on our mapping of the interaction domain important for EBAG9 binding, which includes the N-terminal region of Snapin (aa21-82) and the H1 domain (aa 37-65) residing therein, we hypothesized that the phosphorylation of Snapin at residue S50 might be influenced by the association with EBAG9.

HEK293 cells were cotransfected with Snapin-GFP and EBAG9, followed by metabolic labeling with $^{32}P_i$ and stimulation with the PKC inductor PMA or the PKA inductor Forskolin, respectively. Snapin-GFP received a high basal level of phosphorylation in mock (empty vector) transfected cells, while the cotransfection of EBAG9 decreased the basal phosphorylation of Snapin-GFP significantly (mean 50%, p = 0.016). Unexpectedly, PKA stimulation with Forskolin failed to increase the basal phosphorylation of Snapin (Figure 10A). In our hands, phosphorylation of recombinantly expressed histidine-tagged Snapin by PKA was even less efficient than those obtained for other substrates, including SNAP25 and

Casein (Figure 10B). Analysis of the amino acid sequence of Snapin for potential kinase consensus sites revealed that position S50 can be targeted by PKA, but this site was also identified as a potential target motif for CKII. In an *in vitro* phosphorylation assay, CKII-dependent phosphorylation of Snapin was not seen. We note that the truncated GST-EBAG9 mutant Δ1-30 was phosphorylated in abundance by recombinant PKA and CKII (Figure 10C). In conclusion, in the presence of EBAG9 *in vivo* phosphorylation of Snapin is strongly reduced.

EBAG9 inhibits binding of Snapin to SNAP25 and SNAP23

To explore the functional consequences of Snapin association with EBAG9, a competition study was carried out using immobilized GST-SNAP25 and *in vitro* translated Snapin. This system was supplemented with various amounts of *in vitro* translated EBAG9. Increasing amounts of *in vitro* translated EBAG9 gradually impeded association of Snapin and SNAP25, with a saturation obtained at 25 µl EBAG9 (Figure 11A). Based on the methionine and cysteine content (Snapin: 3; EBAG9: 7) and relative intensity of both molecules analyzed by densitometric scanning of direct loads (Huppa and Ploegh, 1997), a 1:1 stoichiometry was suggested for both molecules.

In a similar experimental approach, EBAG9 inhibited binding of Snapin to SNAP23 (Figure 11B). The modulatory capacity of EBAG9 in the Snapin-SNAP23 interaction strongly suggests a more general role for EBAG9 in membrane fusion events in non-neuronal cells as well.

Discussion

The results presented here are of interest for several aspects of cell biology. First, the identification of Snapin as an interaction partner of EBAG9 allowed us to assess the physiological function of EBAG9 as a highly conserved and ubiquitously expressed protein in mammalian cells. Second, this characterization might point to a putative link between high level expression of EBAG9 in some tumors, exocytosis and the occurrence of tumor-associated O-linked glycans (Akahira *et al.*, 2004; Engelsberg *et al.*, 2003; Tsuneizumi *et al.*, 2001). Few examples of plasma membrane glycoproteins and glycolipids were reported where the Ca^{2+} trigger in regulated exocytosis was also crucial for the levels of plasma membrane receptors and transporters, among them the glucose transporter. Surface deposition is regulated in response to insulin and is mediated by regulated exocytosis (Whitehead *et al.*, 2001). We envisage that EBAG9-mediated modulation of the secretory pathway might favor the deposition of those truncated, normally cryptic glycans at the cell surface. Other examples that link exocytosis and tumor development include the EWS-WT1 gene-fusion product in desmoplasmic small round cell tumors that gives rise to overexpression of the Munc13-1 related molecule BAIAP3. Based on this homology, BAIAP3 was suggested to play a regulatory role in exocytosis (Palmer *et al.*, 2002).

Snapin itself is implicated in synaptic transmission since it binds to SNAP25, mediated through its C-terminal domain (aa79-136) (Ilardi *et al.*, 1999). Although initially considered as a brain specific, synaptic vesicle localized SNARE-complex associated molecule, it has turned out that Snapin is also expressed in non-neuronal cells. Accordingly, Snapin can also form a ternary complex with the non-neuronal isoform of SNAP25, SNAP23 (Buxton *et al.*, 2003). Since we observed a posttranslational membrane association in microsomal membranes and a predominant cytoplasmic staining pattern together with a punctate staining

in the perinuclear region of HEK293 cells, we suggest that Snapin is implicated in vesicle trafficking pathways that are separate from the specialized forms observed at neuronal synapses. In support of this conclusion, inhibition of Snapin binding to the non-neuronal SNAP25 homologue, SNAP23, in the presence of EBAG9 suggests a more general role of EBAG9 and Snapin in membrane fusion events in other cell types. In addition, the identification of other Snapin-interacting proteins expanded the role of Snapin to the biogenesis of lysosome-related organelles and to the cycling and subcellular localization of adenylyl cyclase VI through interactions with the SNARE complex, respectively (Chou *et al.*, 2004; Starcevic and Dell'Angelica, 2004).

The association of EBAG9 with Snapin prompted us to explore a potential modulatory role of EBAG9 in regulated exocytosis. The overexpression of membrane-associated EBAG9 in PC12 cells effectuated a significant reduction in neuropeptide Y and catecholamine release. A modulatory impact on regulated exocytosis, but not on constitutive secretion was suggested by the inability of EBAG9 to alter α1-antitrypsin release from HepG2 cells. These assays supported our notion that the effects of EBAG9 overexpression on regulated secretion were specific, but not due to a severe structural or functional disturbance of the secretory pathway.

The phosphomimetic Snapin mutant, S50D, increased the initial exocytotic burst phase, suggesting that Snapin phosphorylation positively regulates LDCV (Chheda *et al.*, 2001). In contrast, the sustained component of LDCV exocytosis was increased by both mutants, S50D and a S50A variant, the latter mimics an unphosphorylated state. It was inferred that Snapin might act additionally as a priming factor in the presynaptic vesicle cycle (Chheda *et al.*, 2001). The reduction in release of the surrogate neurotransmitter NPY upon overexpression of the Snapin inhibitor EBAG9 is largely in agreement with the suggested function of Snapin in release from LDCV. Our failure to observe an inhibitory effect on evoked neurotransmitter release or size of the RRP in hippocampal neurons might relate to the lack of concomitant overexpression of phosphorylated Snapin as downstream effector molecule for EBAG9

(Thakur *et al.*, 2004). Secondly, several differences between the release machineries in chromaffin cells and neurons have been suggested. Chromaffin cells release catecholamines from LDCVs, whereas hippocampal neurons serve as a model system for release from small clear vesicles. More specifically, differences in pool sizes and kinetic properties have been recorded (Rettig and Neher, 2002). Whereas overexpression of priming factors in chromaffin cells causes large parallel alterations in pool sizes, those changes have not been observed in neurons (Betz *et al.*, 2001).

Since Synaptotagmin I affects exclusively the RRP (Geppert *et al.*, 1994; Voets *et al.*, 2001), the effects of EBAG9 in conjunction with Snapin are unlikely to rest solely on a reduced binding of Synaptotagmin I to the neuronal SNARE complex. Instead, Synaptotagmin III and VII were suggested to play a role during slow/sustained Ca^{2+} triggered exocytosis in PC12 cells, possibly modulated by Snapin and EBAG9 (Südhof, 2002; Sugita *et al.*, 2002). The effects observed for EBAG9 and Snapin would be in agreement with a promiscuous role of Snapin where binding of other Synaptotagmin isoforms to the SNARE complex are controlled as well. In conclusion, we envisage that EBAG9 modulates priming of Synaptotagmin-associated SNARE-complex assembly, as mediated through the linker protein Snapin.

Based on a failure to observe association of Snapin and SNAP25 in biochemical assays and on lack of effects seen for overexpression of a C-terminally truncated variant in neuronal transmission, a recent study suggested a reconsideration of the function of Snapin in neurotransmitter release (Vites *et al.*, 2004). However, in comparison to previous reports (Buxton *et al.*, 2003; Chheda *et al.*, 2001; Ilardi *et al.*, 1999) this novel study did not employ the S50D mutant or injection of C-terminal peptides to explore changes in synaptic transmission and is therefore not directly comparable.

Phosphorylation as a regulatory mechanism acts at different stages of the vesicle cycle, but only few substrates with physiological relevance were identified (Evans and Morgan, 2003; Turner *et al.*, 1999). Our data on the EBAG9-Snapin interaction suggest that inhibition of

Snapin phosphorylation might reduce the association of Snapin with SNAP25 and SNAP23, followed by a decrease in Synaptotagmin recruitment. When we revisited the phosphorylation reaction of Snapin, we failed to observe an enhancement by PMA or Forskolin, which would be expected if PKA or PKC were involved. However, in contrast to a previous report we did not employ back-phosphorylation or the cAMP-analogue BIMP as an inductor of PKA *in vivo* (Chheda *et al.*, 2001).

The intracellular redistribution of EBAG9 upon NGF-induced differentiation in PC12 cells showed a population of molecules that colocalized with the secretory vesicle markers synaptophysin and VAMP2 in neurites and in vesicular structures in the vicinity of the plasma membrane. A differentiation dependent redistribution of vesicle markers has also been reported for Synaptotagmin IV (Fukuda *et al.*, 2003) and hepatocyte growth factor-regulated kinase substrate (Kwong *et al.*, 2000). We suggest that EBAG9 is subject to a dynamic redistribution in differentiated neuroendocrine cells, possibly facilitated by its palmitoylation anchor. Since sorting of proteins is also regulated at the level of protein phosphorylation (Kataoka *et al.*, 2000; Krantz *et al.*, 2000), and EBAG9 was shown to be a substrate for PKA and CKII *in vitro*, this effect could additionally account for the redistribution of EBAG9 in NGF-stimulated PC12 cells. Other phosphorylated SNARE family members that are essential for distinct steps in the regulation of exocytosis include VAMP, Syntaxin, SNAP25, SNAP23, but also the SNARE regulatory molecules Rabphilin 3A and Synaptotagmin (Bennett *et al.*, 1993; Cabaniols *et al.*, 1999; Fykse *et al.*, 1995; Nagy *et al.*, 2004; Nielander *et al.*, 1995; Risinger and Bennett, 1999).

In conclusion, the activity of EBAG9 in regulated exocytosis is mediated via its target molecule Snapin. This relationship adds not only an additional layer of control on the exocytotic machinery, but also advances our mechanistic understanding of a process that requires a tight fine-tuning. In view of this more physiological role, a potential function of EBAG9 in dysregulation of exocytosis in tumor cells requires further studies.

Acknowledgements

We are grateful to Drs. Reinhard Jahn, Mitsunori Fukuda, Wolfhard Almers, and Zu-Hang Sheng for providing fusion protein constructs and Dr. Christian Ried for help in gel filtration. We thank D. Reuter and Ina Herfort for expert technical assistance and the animal facilities of the Max-Planck-Institut für Biophysikalische Chemie. We are grateful to E. Neher for stimulating discussions and continuous support, and Sören Panse, Uta E. Höpken and Kurt Bommert for critical evaluation of the manuscript. This work was supported by a grant from Deutsche Krebshilfe (to A.R.).

References

Akahira, J.-I., Aoki, M., Suzuki, T., Moriya, T., Niikura, H., Ito, K., Inoue, S., Okamura, K., Sasano, H., and Yaegashi, N. (2004). Expression of EBAG9/RCAS1 is associated with advanced disease in human epithelial ovarian cancer. Br. J. Cancer *90*, 2197-2202.

Ashery, U., Betz, A., Xu, T., Brose, N., and Rettig, J. (1999). An efficient method for infection of adrenal chromaffin cells using the Semliki Forest virus gene expression system. Eur. J. Cell Biol. *78*, 525-532.

Bennett, M.K., Miller, K.G., and Scheller, R.H. (1993). Casein kinase II phosphorylates the synaptic vesicle protein p65. J. Neurosci. *13*, 1701-1707.

Betz, A., Thakur, P., Junge, H.J., Ashery, U., Rhee, J.-S., Scheuss, V., Rosenmund, C., Rettig, J., and Brose, N. (2001). Functional Interaction of the Active Zone Proteins Munc13-1 and RIM1 in Synaptic Vesicle Priming. Neuron *30*, 183-196.

Brose, N., Petrenko, A.G., Sudhof, T.C., and Jahn, R. (1992). Synaptotagmin: a calcium sensor on the synaptic vesicle surface. Science *256*, 1021-1025.

Burgess, T.L., and Kelly, R.B. (1987). Constitutive and regulated secretion of proteins. Annu. Rev. Cell Biol. *3*, 243-93.

Burgoyne, R.D., and Morgan, A. (2003). Secretory granule exocytosis. Physiol. Rev. *83*, 581-632.

Buxton, P., Zhang, X.M., Walsh, B., Sriratana, A., Schenberg, I., Manickam, E., and Rowe, T. (2003). Identification and characterization of Snapin as a ubiquitously expressed SNARE-binding protein that interacts with SNAP23 in non-neuronal cells. Biochem. J. *375*, 433-440.

Cabaniols, J.P., Ravichandran, V., and Roche, P.A. (1999). Phosphorylation of SNAP-23 by the novel kinase SNAK regulates t-SNARE complex assembly. Mol. Biol. Cell *10*, 4033-4041.

Chapman, E.R. (2002). Synaptotagmin: a Ca(2+) sensor that triggers exocytosis? Nat. Rev. Mol. Cell Biol. *3*, 498-508.

Chen, Y.A., Scales, S.J., Patel, S.M., Doung, Y.C., and Scheller, R.H. (1999). SNARE complex formation is triggered by Ca2+ and drives membrane fusion. Cell *97*, 165-174.

Chheda, M.G., Ashery, U., Thakur, P., Rettig, J., and Sheng, Z.H. (2001). Phosphorylation of Snapin by PKA modulates its interaction with the SNARE complex. Nat. Cell Biol. *3*, 331-338.

Chilcote, T.J., Galli, T., Mundigl, O., Edelmann, L., McPherson, P.S., Takei, K., and De Camilli, P. (1995). Cellubrevin and synaptobrevins: similar subcellular localization and biochemical properties in PC12 cells. J. Cell Biol. *129*, 219-231.

Chou, J.-L., Huang, C.-L., Lai, H.-L., Hung, A.C., Chien, C.-L., Kao, Y.-Y., and Chern, Y. (2004). Regulation of Type VI Adenylyl Cyclase by Snapin, a SNAP25-binding Protein. J. Biol. Chem. *279*, 46271-46279.

Cichon, G., et al. (1999). Intravenous administration of recombinant adenoviruses causes thrombocytopenia, anemia and erythroblastosis in rabbits. J. Gene Med. *1*, 360-371.

Engelsberg, A., Hermosilla, R., Karsten, U., Schulein, R., Dorken, B., and Rehm, A. (2003). The Golgi protein RCAS1 controls cell surface expression of tumor-associated O-linked glycan antigens. J. Biol. Chem. *278*, 22998-23007.

Evans, G.J., and Morgan, A. (2003). Regulation of the exocytotic machinery by cAMP-dependent protein kinase: implications for presynaptic plasticity. Biochem. Soc. Trans. *31*, 824-827.

Fernandez-Chacon, R., and Südhof, T.C. (1999). Genetics of synaptic vesicle function: toward the complete functional anatomy of an organelle. Annu. Rev. Physiol. *61*, 753-776.

Fukuda, M. (2003). Slp4-a/granuphilin-a inhibits dense-core vesicle exocytosis through interaction with the GDP-bound form of Rab27A in PC12 cells. J. Biol. Chem. *278*, 15390-15396.

Fukuda, M., Kanno, E., Ogata, Y., Saegusa, C., Kim, T., Loh, Y.P., and Yamamoto, A. (2003). Nerve growth factor-dependent sorting of synaptotagmin IV protein to mature dense-core vesicles that undergo calcium-dependent exocytosis in PC12 cells. J. Biol. Chem. *278*, 3220-3226.

Fykse, E.M., Li, C., and Sudhof, T.C. (1995). Phosphorylation of rabphilin-3A by Ca2+/calmodulin- and cAMP-dependent protein kinases in vitro. J. Neurosci. *15*, 2385-2395.

Geppert, M., Goda, Y., Hammer, R.E., Li, C., Rosahl, T.W., Stevens, C.F., and Sudhof, T.C. (1994). Synaptotagmin I: a major Ca2+ sensor for transmitter release at a central synapse. Cell *79*, 717-727.

Gieselmann, V., Pohlmann, R., Hasilik, A., and Von_Figura, K. (1983). Biosynthesis and transport of cathepsin D in cultured human fibroblasts. J. Cell Biol. *97*, 1-5.

Huppa, J.B., and Ploegh, H.L. (1997). In vitro translation and assembly of a complete T cell receptor-CD3 complex. J. Exp. Med. *186*, 393-403.

Ikeda, K., Sato, M., Tsutsumi, O., Tsuchiya, F., Tsuneizumi, M., Emi, M., Imoto, I., Inazawa, J., Muramatsu, M., and Inoue, S. (2000). Promoter Analysis and Chromosomal Mapping of Human EBAG9 Gene. Biochem. Biophys. Res. Commun. *273*, 654-660.

Ilardi, J.M., Mochida, S., and Sheng, Z.H. (1999). Snapin: a SNARE-associated protein implicated in synaptic transmission. Nat. Neurosci. *2*, 119-124.

Jahn, R., and Südhof, T.C. (1999). Membrane fusion and exocytosis. Annu. Rev. Biochem. *68*, 863-911.

Kataoka, M., Kuwahara, R., Iwasaki, S., Shoji-Kasai, Y., and Takahashi, M. (2000). Nerve growth factor-induced phosphorylation of SNAP-25 in PC12 cells: a possible involvement in the regulation of SNAP-25 localization. J. Neurochem. *74*, 2058-2066.

Koticha, D.K., Huddleston, S.J., Witkin, J.W., and Baldini, G. (1999). Role of the cysteine-rich domain of the t-SNARE component, SYNDET, in membrane binding and subcellular localization. J. Biol. Chem. *274*, 9053-9060.

Krantz, D.E., Waites, C., Oorschot, V., Liu, Y., Wilson, R.I., Tan, P.K., Klumperman, J., and Edwards, R.H. (2000). A phosphorylation site regulates sorting of the vesicular acetylcholine transporter to dense core vesicles. J. Cell Biol. *149*, 379-396.

Kubokawa, M., Nakashima, M., Yao, T., Ito, K.I., Harada, N., Nawata, H., and Watanabe, T. (2001). Aberrant intracellular localization of RCAS1 is associated with tumor progression of gastric cancer. Int. J. Oncology *19*, 695-700.

Kwong, J., Roundabush, F.L., Hutton-Moore, P., Montague, M., Oldham, W., Li, Y., Chin, L.S., and Li, L. (2000). Hrs interacts with SNAP-25 and regulates Ca(2+)-dependent exocytosis. J. Cell Sci. *113 (Pt 12)*, 2273-2284.

Leelawat, K., Watanabe, T., Nakajima, M., Tujinda, S., Suthipintawong, C., and Leardkamolkarn, V. (2003). Upregulation of tumour associated antigen RCAS1 is implicated in high stages of colorectal cancer. J. Clin. Pathol. *56*, 764-768.

Lupas, A., Van-Dyke, M., and Stock, J. (1991). Predicting coiled coils from protein sequences. Science *252*, 1162-1164.

Matveeva, E.A., Whiteheart, S.W., and Slevin, J.T. (2003). Accumulation of 7S SNARE complexes in hippocampal synaptosomes from chronically kindled rats. J. Neurochem. *84*, 621-624.

Nagy, G., Reim, K., Matti, U., Brose, N., Binz, T., Rettig, J., Neher, E., and Sorensen, J.B. (2004). Regulation of releasable vesicle pool sizes by protein kinase A-dependent phosphorylation of SNAP-25. Neuron *41*, 417-429.

Nielander, H.B., Onofri, F., Valtorta, F., Schiavo, G., Montecucco, C., Greengard, P., and Benfenati, F. (1995). Phosphorylation of VAMP/synaptobrevin in synaptic vesicles by endogenous protein kinases. J. Neurochem. *65*, 1712-1720.

Palmer, R.E., Lee, S.B., Wong, J.C., Reynolds, P.A., Zhang, H., Truong, V., Oliner, J.D., Gerald, W.L., and Haber, D.A. (2002). Induction of BAIAP3 by the EWS-WT1 chimeric fusion implicates regulated exocytosis in tumorigenesis. Cancer Cell *2*, 497-505.

Rehm, A., and Ploegh, H.L. (1997). Assembly and intracellular targeting of the betagamma subunits of heterotrimeric G proteins. J. Cell Biol. *137*, 305-317.

Reim, K., Mansour, M., Varoqueaux, F., McMahon, H.T., Sudhof, T.C., Brose, N., and Rosenmund, C. (2001). Complexins regulate a late step in Ca2+-dependent neurotransmitter release. Cell *104*, 71-81.

Rettig, J., and Neher, E. (2002). Emerging roles of presynaptic proteins in Ca++-triggered exocytosis. Science *298*, 781-785.

Risinger, C., and Bennett, M.K. (1999). Differential phosphorylation of syntaxin and synaptosome-associated protein of 25 kDa (SNAP-25) isoforms. J. Neurochem. *72*, 614-624.

Rosenmund, C., and Stevens, C.F. (1996). Definition of the readily releasable pool of vesicles at hippocampal synapses. Neuron *16*, 1197-1207.

Shin, O.-H., Maximov, A., Lim, B.K., Rizo, J., and Sudhof, T.C. (2004). Unexpected Ca2+-binding properties of synaptotagmin 9. Proc. Natl. Acad. Sci. U S A *101*, 2554-2559.

Smith, D.B., and Johnson, K.S. (1988). Single-step purification of polypeptides expressed in Escherichia coli as fusions with glutathione S-transferase. Gene *67*, 31-40.

Söllner, T., Whiteheart, S.W., Brunner, M., Erdjument_Bromage, H., Geromanos, S., Tempst, P., and Rothman, J.E. (1993). SNAP receptors implicated in vesicle targeting and fusion. Nature *362*, 318-324.

Starcevic, M., and Dell'Angelica, E.C. (2004). Identification of snapin and three novel proteins (BLOS1, BLOS2, and BLOS3/reduced pigmentation) as subunits of biogenesis of lysosome-related organelles complex-1 (BLOC-1). J. Biol. Chem. *279*, 28393-28401.

Südhof, T.C. (1995). The synaptic vesicle cycle: a cascade of protein-protein interactions. Nature *375*, 645-653.

Südhof, T.C. (2002). Synaptotagmins: why so many? J. Biol. Chem. *277*, 7629-7632.

Sugita, S., Shin, O.H., Han, W., Lao, Y., and Sudhof, T.C. (2002). Synaptotagmins form a hierarchy of exocytotic Ca(2+) sensors with distinct Ca(2+) affinities. EMBO J. *21*, 270-280.

Sutton, R.B., Fasshauer, D., Jahn, R., and Brunger, A.T. (1998). Crystal structure of a SNARE complex involved in synaptic exocytosis at 2.4 A resolution. Nature *395*, 347-353.

Suzuki, T., Inoue, S., Kawabata, W., Akahira, J., Moriya, T., Tsuchiya, F., Ogawa, S., Muramatsu, M., and Sasano, H. (2001). EBAG9/RCAS1 in human breast carcinoma: a possible factor in endocrine-immune interactions. Br. J. Cancer *85*, 1731-1737.

Thakur, P., Stevens, D.R., Sheng, Z.-H., and Rettig, J. (2004). Effects of PKA-mediated phosphorylation of Snapin on synaptic transmission in cultured hippocampal neurons. J. Neurosci. *24*, 6476-6481.

Tsuchiya, F., Ikeda, K., Tsutsumi, O., Hiroi, H., Momoeda, M., Taketani, Y., Muramatsu, M., and Inoue, S. (2001). Molecular cloning and characterization of mouse EBAG9, homolog of a human cancer associated surface antigen: expression and regulation by estrogen. Biochem. Biophys. Res. Commun. *284*, 2-10.

Tsuneizumi, M., Emi, M., Nagai, H., Harada, H., Sakamoto, G., Kasumi, F., Inoue, S., Kazui, T., and Nakamura, Y. (2001). Overrepresentation of the EBAG9 gene at 8q23 associated with early-stage breast cancers. Clin. Cancer Res. *7*, 3526-3532.

Turner, K.M., Burgoyne, R.D., and Morgan, A. (1999). Protein phosphorylation and the regulation of synaptic membrane traffic. Trends Neurosci. *22*, 459-464.

Vites, O., Rhee, J.-S., Schwarz, M., Rosenmund, C., and Jahn, R. (2004). Reinvestigation of the role of snapin in neurotransmitter release. J. Biol. Chem. *279*, 26251-26256.

Voets, T., Moser, T., Lund, P.E., Chow, R.H., Geppert, M., Sudhof, T.C., and Neher, E. (2001). Intracellular calcium dependence of large dense-core vesicle exocytosis in the absence of synaptotagmin I. Proc. Natl. Acad. Sci. U S A *98*, 11680-11685.

Wang, C.T., Grishanin, R., Earles, C.A., Chang, P.Y., Martin, T.F., Chapman, E.R., and Jackson, M.B. (2001). Synaptotagmin modulation of fusion pore kinetics in regulated exocytosis of dense-core vesicles. Science *294*, 1111-1115.

Weber, E., Jilling, T., and Kirk, K. (1996). Distinct functional properties of Rab3A and Rab3B in PC12 neuroendocrine cells. J. Biol. Chem. *271*, 6963-6971.

Whitehead, J.P., Molero, J.C., Clark, S., Martin, S., Meneilly, G., and James, D.E. (2001). The role of Ca2+ in insulin-stimulated glucose transport in 3T3-L1 cells. J. Biol. Chem. *276*, 27816-27824.

Figure Legends

Figure 1. Yeast two-hybrid studies of EBAG9 interacting clones

(A) Screening of a human brain cDNA library allowed the identification of nine EBAG9 interacting clones. Clones 7 and 6B showed strongest lacZ reporter activation and encoded full length Snapin. The positive control is represented by a clone consisting of BD-p53 and AD-SV40 T-antigen. The combination BD-EBAG9 and AD-SV40 T-antigen provided the negative control (0%). β-galactosidase activity is expressed as percentage of the positive control. Data represent the mean values ± S.D. of three independent transformants.

(B) Specificity of EBAG9-Snapin association. Yeast cells were cotransformed with the indicated GAL4 DNA-binding domain (BD) and GAL4 activation domain (AD) plasmids. The unrelated bait BD-Lamin C represented an additional negative control. Colonies were screened for interaction by their ability to grow in the absence of histidine and adenine and by α-galactosidase activity (Mel1). -, no interaction; +++, strong interaction.

Figure 2. EBAG9 interacts with Snapin *in vitro* and *in vivo*

(A) GST-Snapin, GST-SNAP25, GST-VAMP2 or GST (3 μg each) immobilized on glutathione-sepharose beads were incubated with *in vitro* translated [^{35}S] labeled EBAG9. Bound proteins were analyzed by 12.5% SDS-PAGE and autoradiography (upper panel). An aliquot was separated by SDS-PAGE and stained with Coomassie blue to control equal load of various GST fusion proteins (lower panel, Input GST). To score for the amount of *in vitro* translated EBAG9 (Input EBAG9), one quarter of the translation mix was resolved by SDS-PAGE (upper panel).

(B) HEK293 cells were transiently transfected with Snapin-GFP, solubilized in TX-100 containing lysis buffer and cell lysate was then incubated with immobilized GST-fusion proteins, as indicated. Bound proteins were resolved by SDS-PAGE and transferred to nitrocellulose. Immunodetection of Snapin-GFP (IB) was done with biotinylated anti-GFP antibody (upper panel). After stripping, the same membranes were probed with anti-GST antibody to confirm comparable loading of GST-fusion proteins (lower panel).

(C) HEK293 cells were transfected with Snapin-GFP, N-Flag-EBAG9 or both. Cells were lysed in TX-100 containing lysis buffer and immunoprecipitations (IP) were carried out with anti-Flag mAb M5. Immunoprecipitates were analyzed by SDS-PAGE, followed by immunoblotting with biotinylated anti-GFP antibody (top panel). In the middle panel, an aliquot (1/40) of the cell lysate was assessed for the expression of recombinant EBAG9, employing a polyclonal anti-EBAG9 serum for immunoblotting (IB). In the bottom panel, the amount of Snapin-GFP in the starting material was determined using an anti-GFP antibody.

(D) Cell lysates of HEK293 cells transfected with EBAG9-C-Flag, Snapin-GFP or both were processed as shown in (C) and immunoprecipitated with rabbit anti-GFP serum. Coimmunoprecipitated EBAG9-C-Flag was detected in immunoblot (IB) with anti-Flag mAb M2 (top panel). Snapin-GFP was detected with biotinylated anti-GFP antibody (bottom panel, input Snapin), the middle panel shows EBAG9-C-Flag expressed in cell lysates.

(E) Size exclusion chromatography. PC12 cells were lysed in CHAPS-containing lysis buffer, followed by separation on a Superdex 200 gel filtration column as described under “Materials and methods". Fractions were analyzed by SDS-PAGE and immunoblotting for EBAG9 and Snapin. The positions of molecular weight standards and the exclusion volume (V_o) are indicated.

Figure 3. Mapping of the interaction sites between EBAG9 and Snapin

(A) Snapin associates with EBAG9 via its predicted N-terminal coiled-coil domain. Lysates of EBAG9-GFP transfected HEK293 cells were incubated with the indicated GST-Snapin deletion mutants or the Snapin S50D mutant. Complexes were washed in CHAPS-containing lysis buffer, and bound EBAG9-GFP was analyzed by SDS-PAGE and immunoblotting (IB) using biotinylated anti-GFP antibody (upper panel). Blots were stripped and reprobed with anti-GST antibody to ensure equivalent loading of GST proteins (lower panel). Input EBAG9-GFP, 1/40 volume of the reaction mixture used for each pulldown.

On the right, a schematic representation of GST-Snapin and its deletion mutants. The GST tag, the predicted hydrophobic domain (HD) and two predicted coiled-coil domains (H1 and H2).

(B) EBAG9 binds to Snapin via its predicted TM-region. EBAG9 mutants were expressed and analyzed as shown in (A). The putative transmembrane domain alone (EBAG9 Δ30-213-GFP) was sufficient to associate with Snapin wt or Snapin aa 21-82, exhibiting the H1 domain. In the middle panel, an aliquot (1/40 volume) of the cell lysates was assessed by immunoblotting (IB) for the expression of equal amounts of EBAG9-GFP truncated variants. Bottom, input GST-Snapin fusion protein.

On the right, a schematic representation of EBAG9-GFP and its deletion mutants. TM, the predicted transmembrane region (aa 8-27); CC, coiled-coil domain (aa 179-206).

Figure 4. Palmitoylation contributes to membrane association of EBAG9

(A) HEK293 cells were transiently transfected with wt EBAG9-GFP (right panel), or with a cysteine deficient mutant (C12/14/17S) (left panel) and were analyzed by confocal microscopy. Scale bar, 20 μm.

(B) HEK293 cells were transfected with EBAG9-GFP, EBAG9 C12/14/27S-GFP, EBAG9 Δ1-27-GFP, followed by metabolic labeling with [^{3}H] palmitic acid for 4 h. Cell lysates were

subjected to immunoprecipitation with anti-GFP serum (IP) and analyzed by SDS-PAGE and autoradiography (upper panel). An aliquot (1/5) of the immunoprecipitates were immunoblotted (IB) with biotinylated anti-GFP antibody.

(C) Aliquots of identical [^{3}H] palmitate labeled EBAG9-GFP immunoprecipitates were resolved by SDS-PAGE and treated separately overnight with 1M Tris or 1M hydroxylamine before autoradiography.

Figure 5. Intracellular distribution of Snapin-GFP

(A) Snapin mRNA was *in vitro* translated in the presence of [^{35}S] methionine/cysteine with (+) or without microsomes (–). Translation was stopped by addition of sample buffer and boiling. Total loads were analyzed by SDS-PAGE and autoradiography.

(B) Snapin associates with microsomal membranes co- or posttranslationally. Microsomes were added to the *in vitro* translation reaction either at the beginning of translation (–) or after induction of translation arrest by inclusion of cycloheximide (+) (10 μg/ml). Microsomes were pelleted, washed twice with PBS and analyzed as shown before.

(C) HEK293 cells were cotransfected with Snapin-GFP (left, green) and pcDNA-EBAG9. Cells were stained with anti-EBAG9 polyclonal serum (middle panel). Secondary goat anti-rabbit antibody and Streptavidin-conjugated Alexa Fluor 568 were used to detect staining of the primary polyclonal antibody (red). Images were analyzed by confocal microscopy, merged images are shown on the right (yellow). Scale bar, 10 μm.

Figure 6. NGF-dependent subcellular redistribution of EBAG9 in PC12 cells

(A) PC12 cells were transiently transfected with EBAG9-GFP and cultured in the absence (–) or presence (+) of NGF for 72h. Cells were fixed, permeabilized and then stained with an anti-Synaptophysin or VAMP2 antibody. Subcellular distribution of EBAG9-GFP (green) and

Synaptophysin or (B), VAMP2 (red) was analyzed by confocal microscopy. Merged images are shown on the right. EBAG9-GFP redistributed from perinuclear regions to vesicular structures and to neurite extensions after NGF treatment. A partial colocalization of EBAG9-GFP with the secretory vesicle markers Synaptophysin and VAMP2 in neurites of differentiated PC12 cells was obtained (merge: yellow). Scale bar, 10 μm.

C) Magnification of overlayed EBAG9-GFP and VAMP2 in neurite extension and intracellular region. The fluorescence intensities measured along a line show amounts of EBAG9-GFP and VAMP2. The fluorescence intensities were plotted as number of pixels (Y-axis) relative to their position along the region (X-axis).

Figure 7. EBAG9 cofractionates with secretory vesicle markers

(A) A postnuclear supernatant (PNS) of NGF-induced PC12 cells was separated by a discontinuous sucrose density gradient and fractions were taken from the top. Protein was precipitated with TCA and analyzed by SDS-PAGE and immunoblotting using the antibodies indicated. Fraction 1, top.

(B) Protein marker distribution was quantified by densitometric scanning and expressed as percentage of the total amount present in the PNS.

Figure 8. Membrane-bound EBAG9 inhibits regulated exocytosis in PC12 cells, while constitutive secretion is unaffected

(A) PC12 cells were cotransfected with NPY-GST and EBAG9-GFP, GFP (mock) or EBAG9 C12/14/27S (C/S). NPY-GST secretion was stimulated by a 10 min incubation with high KCl solution (56 mM) or low KCl solution (5.6mM). Released NPY-GST was captured with glutathione-sepharose beads, and protein bound was analyzed by SDS-PAGE and

immunoblotting. Results are expressed as percentage of NPY-GST secretion, compared to total cellular NPY-GST. Bars, means ± S.D. of three independent experiments. **, p = 0.00025, Student´s unpaired *t* test.

(B) HepG2 cells were infected with Ad-EBAG9-GFP or Ad-GFP (mock) as a control at MOIs between 5-20 for 2 h. After 36 h, cells were labeled with [^{35}S] methionine/cysteine for 10 min, followed by a chase in complete medium. After the indicated periods of chase, α1-antitrypsin was immunoprecipitated and analyzed as detailed in "Materials and Methods". α1-antitrypsin secreted is expressed as percentage of total content. Data are means ± S.D. of a single representative experiment performed in duplicate. Experiments were performed three times.

Figure 9. Basal parameters of synaptic transmission, synaptic amplitudes, and readily releasable vesicle pools

(A) Bar diagram summarizing average synaptic EPSC amplitudes for EBAG9-GFP (+EBAG9) and eGFP (+eGFP) overexpressing neurons. Data are presented ± S.E.M. Values of n indicate total number of cells.

(B) Bar diagram showing the average size of the charge induced by application of 500 mM sucrose during 4 seconds corresponding to the readily releasable pool (RRP). Data and groups are represented as above.

(C) Average EPSC amplitude normalized to the first response during application of 50 stimuli at 10 Hz. Data and groups are represented as above.

Figure 10. EBAG9 inhibits phosphorylation of Snapin

(A) HEK293 cells were transiently cotransfected with Snapin-GFP and pcDNA-EBAG9 or empty vector (mock). Cells were labeled with $^{32}P_i$ and stimulated with PMA (30 ng/ml),

Forskolin (40 µM) or remained unstimulated (none) for 10 min at 37 °C. Snapin-GFP was immunoprecipitated from a detergent lysate with rabbit anti-GFP serum. Immunoprecipitates were analyzed by SDS-PAGE and autoradiography. Snapin-GFP phosphorylation was quantified using BAS 2000 image analyzer and expressed as percentage of [^{32}P] incorporation, as compared to unstimulated, mock-transfected cells (100%). Snapin-GFP phosphorylation levels were normalized to protein loads as assessed by immunoblotting (data not shown). Note that neither PMA nor Forskolin are able to enhance phosphorylation of Snapin-GFP, compared to unstimulated cells. Data represent means ± S.D. of three independent experiments. *, p = 0.0156, Student´s unpaired *t* test**.**

(B) Snapin is an inefficient substrate for recombinant protein kinase A (PKA) and (C), for casein kinase II (CKII). Casein and recombinant proteins GST-SNAP25 (SNAP25), GST-EBAG9 Δ1-30 (ΔEBAG9) and His_6-Snapin (Snapin) (2 µg each) were tested for their ability to receive phosphorylation by PKA (1U/µl) or CKII (1U/µl) *in vitro*. Enzymes were preincubated for 10 min at 30°C with 80 µM ATP in 25 µl of kinase buffer. 2 µCi [γ-^{32}P]ATP was added to the proteins, and reactions were continued for 30 min at 30°C. Reaction products were analyzed by SDS-PAGE. Phosphorylation levels (Casein=100%) were quantified by phosphorscreen and normalized to equimolar protein amounts, as determined by Coomassie Brilliant Blue staining. Data represent the mean values ± S.D. of three independent experiments.

Figure 11. EBAG9 prevents association of Snapin with SNAP25 and SNAP23

(A) A constant amount of immobilized GST-SNAP25 (10 µg) was incubated with a constant amount of *in vitro* translated [^{35}S] labeled Snapin. Increasing amounts of [^{35}S] labeled EBAG9, as obtained from *in vitro* translation, were added. Samples were washed extensively,

and bound Snapin was detected by autoradiography. The amount of Snapin bound to GST-SNAP25 was quantified and expressed in percentage of Snapin bound to SNAP25 without inclusion of EBAG9 (control, 100%). Mock control, reticulocyte lysate that lacks EBAG9.
(B) Likewise, inhibition of Snapin binding to GST-SNAP23 (10 μg) was determined in the presence of EBAG9. Data are representative of four independent experiments in (A) and (B).

Figure Legends: Supplementary Information

Supplementary Information S2. GST-Snapin specifically interacts with *in vitro* translated EBAG9

The indicated GST fusion proteins immobilized on glutathione-sepharose were incubated with *in vitro* translated MHC class I heavy chain (HLA-A3), Snapin or EBAG9. After extensive washing with binding buffer, proteins bound to the beads were analyzed by SDS-PAGE and autoradiograpy. ΔEBAG9, GST-EBAG9 Δ1-30 lacking the membrane proximal domain.

Supplementary Information S3. Coexpression of Snapin rescues inhibition of exocytosis in PC12 cells upon EBAG9 overexpression

[^{3}H]Norepinephrine (NE) release from intact PC12 cells was essentially performed as described (Weber *et al.*, 1996). Briefly, PC12 cells were transfected with 8 µg GFP (mock), EBAG9 Δ30-213-GFP, EBAG9-GFP or were cotransfected with EBAG9-GFP and 4 µg histidine-tagged Snapin (Snapin). Cells were labeled overnight with [^{3}H]NE and stimulated with control solution (5.6 mM KCl) or with 56 mM KCl solution for 10 min. [^{3}H]NE release was determined by liquid scintillation in a ß-counter and normalized to total cell counts. Normalized evoked NE release was calculated as the difference of secretion between control and depolarizing solution and is expressed as percentage of mock transfected cells (Shin *et al.*, 2004). Likewise, statistical significance is based on the significant difference in release between mock transfected and EBAG9-GFP ($p=0.0096$) or EBAG9 Δ30-213-GFP ($p=0.041$) transfected cells. In contrast, upon coexpression of EBAG9 and Snapin this difference in release disappears ($p=0.688$). Expression levels of EBAG9-GFP were comparable in each experiment as assessed by immunoblotting (data not shown). We note that overexpression of the minimal Snapin binding domain of EBAG9 (EBAG9 Δ30-213-GFP) also abolished evoked NE release. Data are means ± S.D of three independent experiments performed in duplicate.

Supplementary Information S4. Acquisition of Endo H resistance of MHC class I heavy chains is not affected by EBAG9 overexpression

Applying pulse-chase analysis, the ER-Golgi transport was measured by tracking the extent of conversion of ER- and cis-Golgi located, Endo H-sensitive MHC class I heavy chain (HC) into the Endo H-resistant Golgi form.

HeLa cells were transfected with EBAG9-GFP or GFP (mock) and labeled with [^{35}S] methionine/cysteine for 10 min, followed by a chase in complete medium. After the indicated periods of chase, MHC class I HC was immunoprecipitated, subjected to Endo H digestion and analyzed by SDS-PAGE and autoradiography. Data are plotted as a percentage of Endo H-resistant MHC class I HC (means ± S.D. of three independent experiments).

Supplementary Information S5. EBAG9 overexpression has no effect on cathepsin D trafficking

Maturation of cathepsin D occurs following delivery of the precursor (53 kD) from the Golgi complex to lysosomes, where it is processed into a 47 kD intermediate (Gieselmann *et al.*, 1983).

EBAG9-GFP or GFP (mock) overexpressing HEK293 cells were metabolically labeled with [^{35}S] methionine/cysteine for 30 min and chased for the indicated times. Immunoprecipitates of cathepsin D were analyzed by SDS-PAGE followed by autoradiograpy. One representative experiment out of three is shown.

Abbreviations

EBAG9, estrogen receptor-binding fragment-associated gene9

LDCV, large dense-core vesicles

NPY, neuropeptide Y

PKA, Protein kinase A

RRP, readily releasable pool of vesicles

SNAP25, synaptosome-associated protein of 25 kd

VAMP, vesicle-associated membrane protein

Figure 1

A

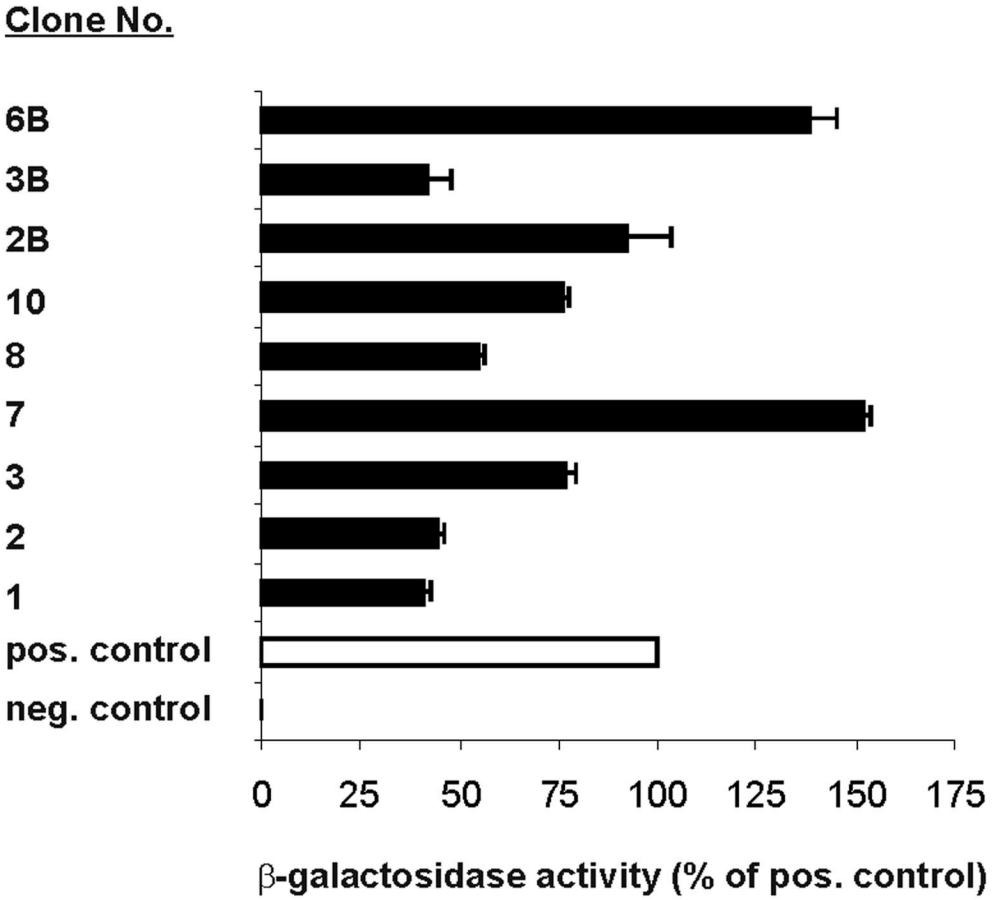

B

bait (BD-)	*prey* (AD-)	interaction
Lamin C	SV40 T-antigen	-
p53	SV40 T-antigen	+++
EBAG9	empty vector	-
EBAG9	SV40 T-antigen	-
EBAG9	Snapin	+++
empty vector	Snapin	-
Lamin C	Snapin	-

Figure 2

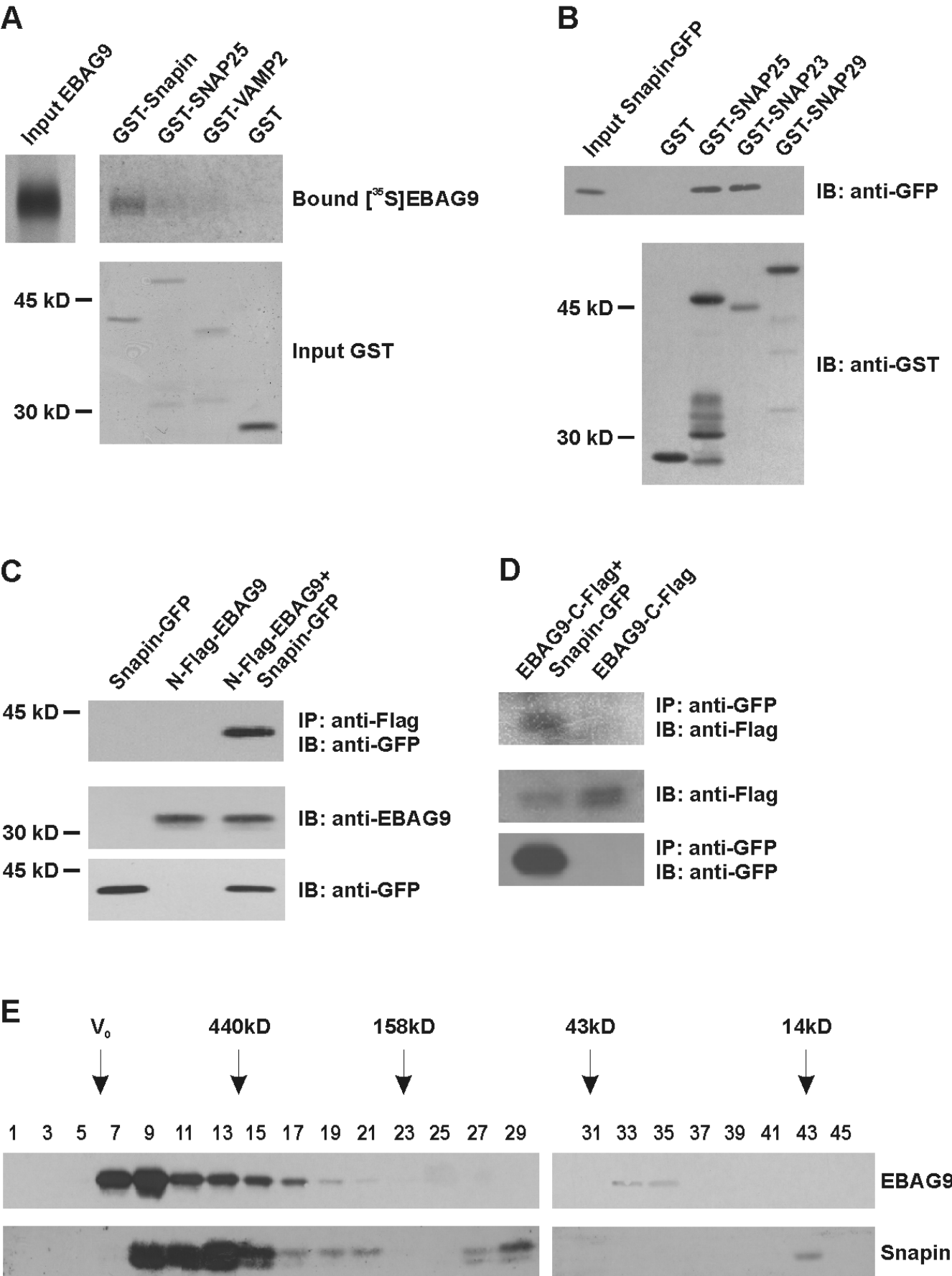
A
Input EBAG9
GST-Snapin
GST-SNAP25
GST-VAMP2
GST
Bound [35S]EBAG9
45 kD
30 kD
Input GST
B
Input Snapin-GFP
GST
GST-SNAP25
GST-SNAP23
GST-SNAP29
IB: anti-GFP
45 kD
30 kD
IB: anti-GST
C
Snapin-GFP
N-Flag-EBAG9
N-Flag-EBAG9+ Snapin-GFP
45 kD
IP: anti-Flag
IB: anti-GFP
30 kD
IB: anti-EBAG9
45 kD
IB: anti-GFP
D
EBAG9-C-Flag+ Snapin-GFP
EBAG9-C-Flag
IP: anti-GFP
IB: anti-Flag
IB: anti-Flag
IP: anti-GFP
IB: anti-GFP
E
V0
440kD
158kD
43kD
14kD
1 3 5 7 9 11 13 15 17 19 21 23 25 27 29
31 33 35 37 39 41 43 45
EBAG9
Snapin

Figure 3

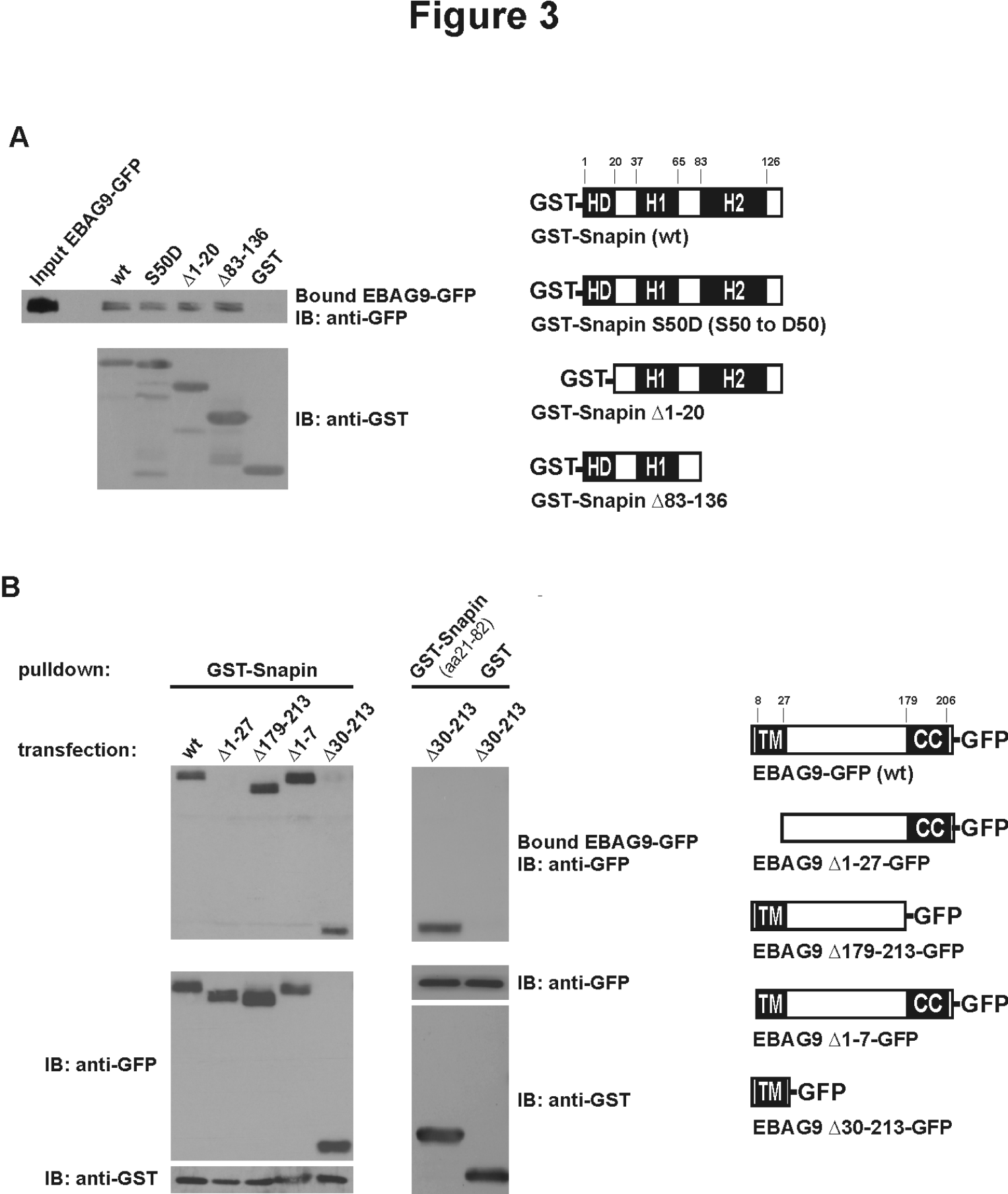
A
Input EBAG9-GFP
wt
S50D
Δ1-20
Δ83-136
GST
Bound EBAG9-GFP
IB: anti-GFP
IB: anti-GST
1
20
37
65
83
126
GST-HD H1 H2
GST-Snapin (wt)
GST-HD H1 H2
GST-Snapin S50D (S50 to D50)
GST-H1 H2
GST-Snapin Δ1-20
GST-HD H1
GST-Snapin Δ83-136
B
pulldown:
GST-Snapin
GST-Snapin (aa21-82)
GST
transfection:
wt
Δ1-27
Δ179-213
Δ1-7
Δ30-213
Δ30-213
Δ30-213
Bound EBAG9-GFP
IB: anti-GFP
IB: anti-GFP
IB: anti-GFP
IB: anti-GST
IB: anti-GST
8
27
179
206
TM CC GFP
EBAG9-GFP (wt)
CC GFP
EBAG9 Δ1-27-GFP
TM GFP
EBAG9 Δ179-213-GFP
TM CC GFP
EBAG9 Δ1-7-GFP
TM GFP
EBAG9 Δ30-213-GFP

Figure 4

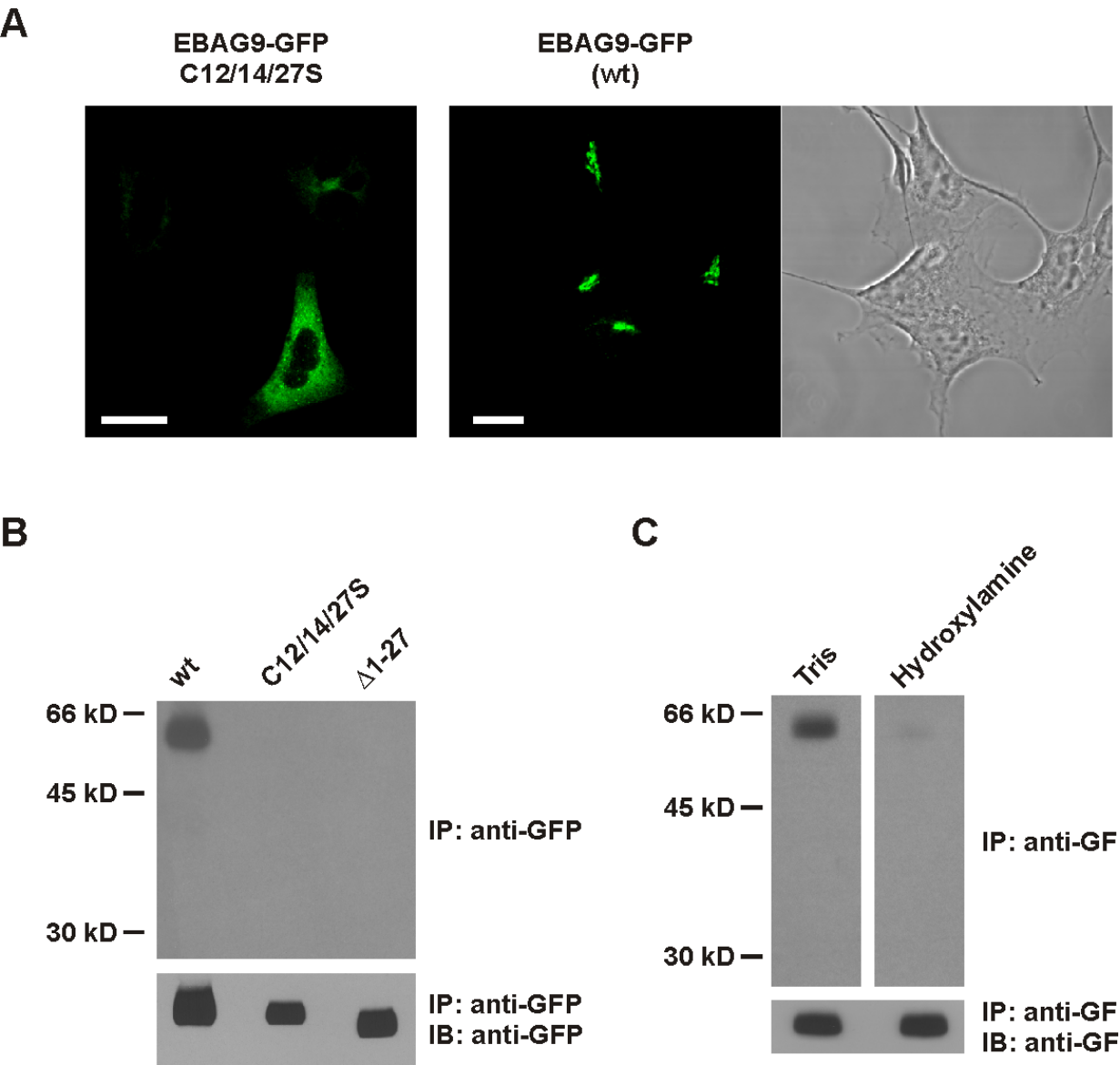
A
EBAG9-GFP
C12/14/27S
EBAG9-GFP
(wt)
B
wt
C12/14/27S
Δ1-27
66 kD
45 kD
30 kD
IP: anti-GFP
IP: anti-GFP
IB: anti-GFP
C
Tris
Hydroxylamine
66 kD
45 kD
30 kD
IP: anti-GFP
IP: anti-GFP
IB: anti-GFP

Figure 5

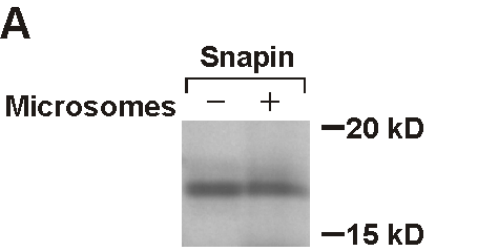
A
Snapin
Microsomes
–
+
20 kD
15 kD

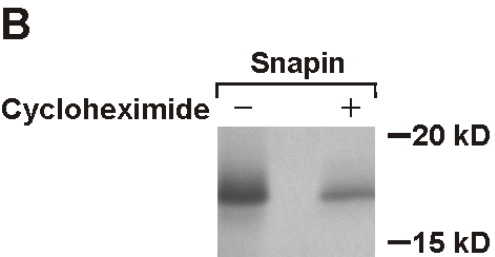
B
Snapin
Cycloheximide
–
+
20 kD
15 kD

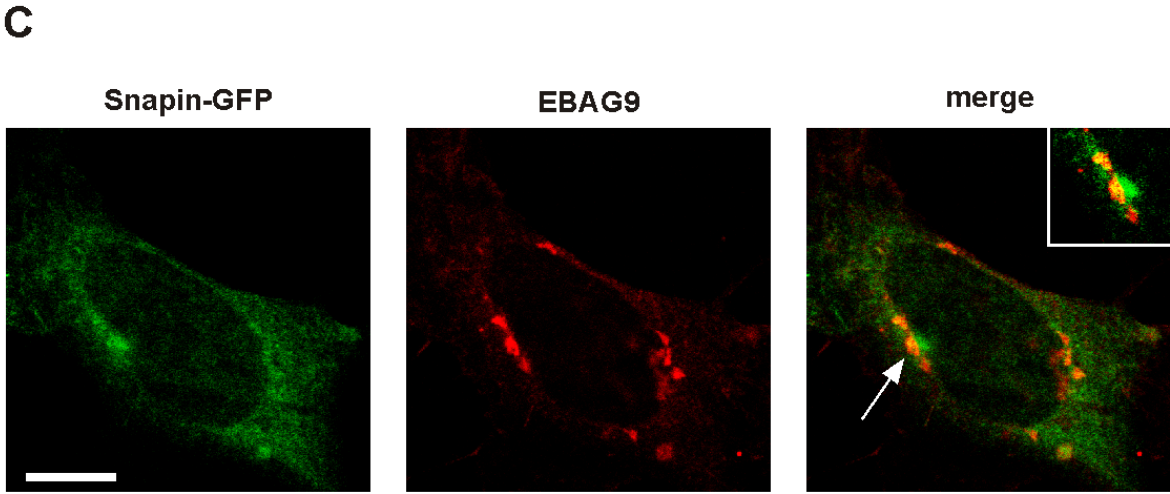
C
Snapin-GFP
EBAG9
merge

Figure 6

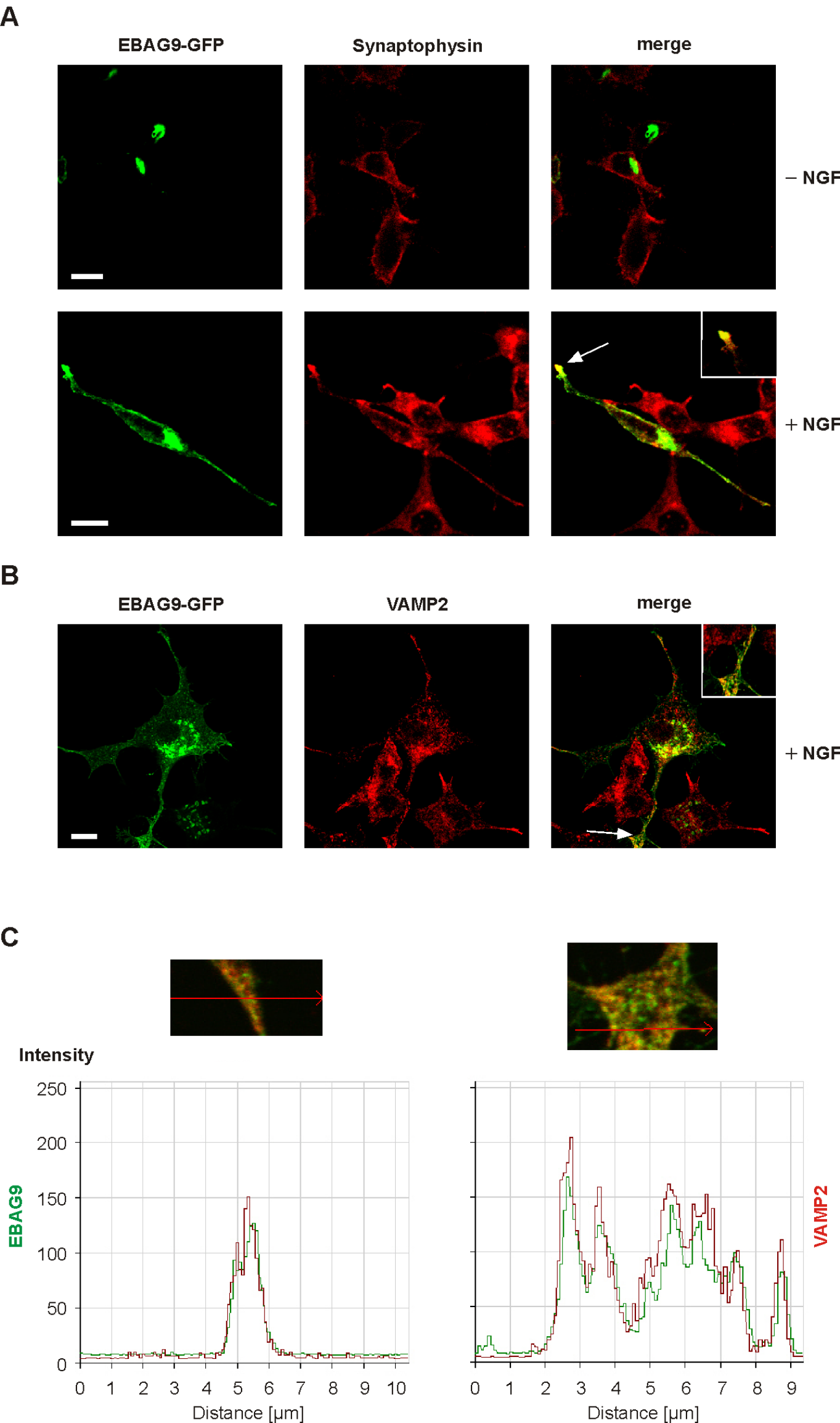
A
EBAG9-GFP
Synaptophysin
merge
– NGF
+ NGF
B
EBAG9-GFP
VAMP2
merge
+ NGF
C
Intensity
EBAG9
VAMP2
250
200
150
100
50
0
0 1 2 3 4 5 6 7 8 9 10
Distance [µm]
0 1 2 3 4 5 6 7 8 9
Distance [µm]

Figure 7

A

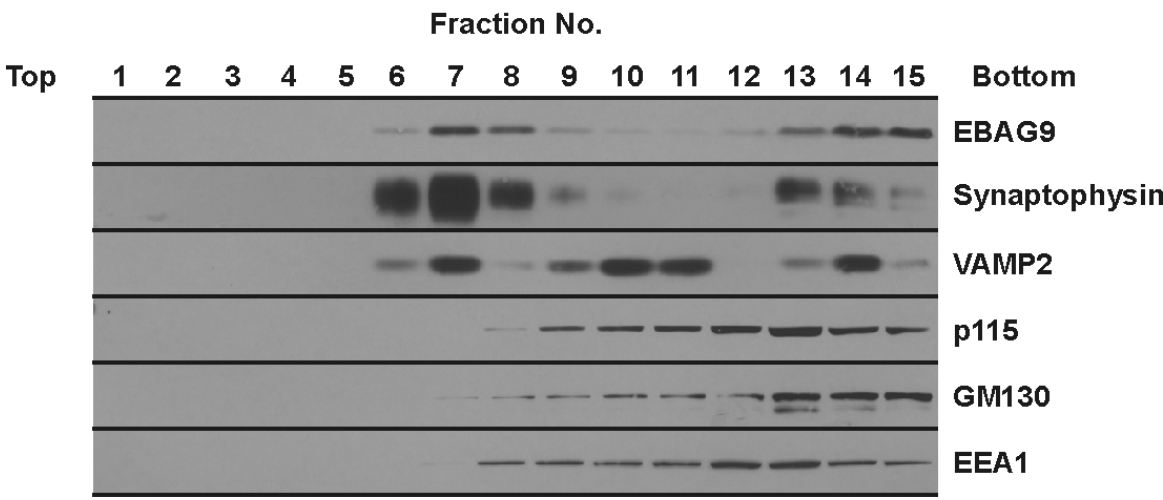
Fraction No.
Top
1 2 3 4 5 6 7 8 9 10 11 12 13 14 15
Bottom
EBAG9
Synaptophysin
VAMP2
p115
GM130
EEA1

B

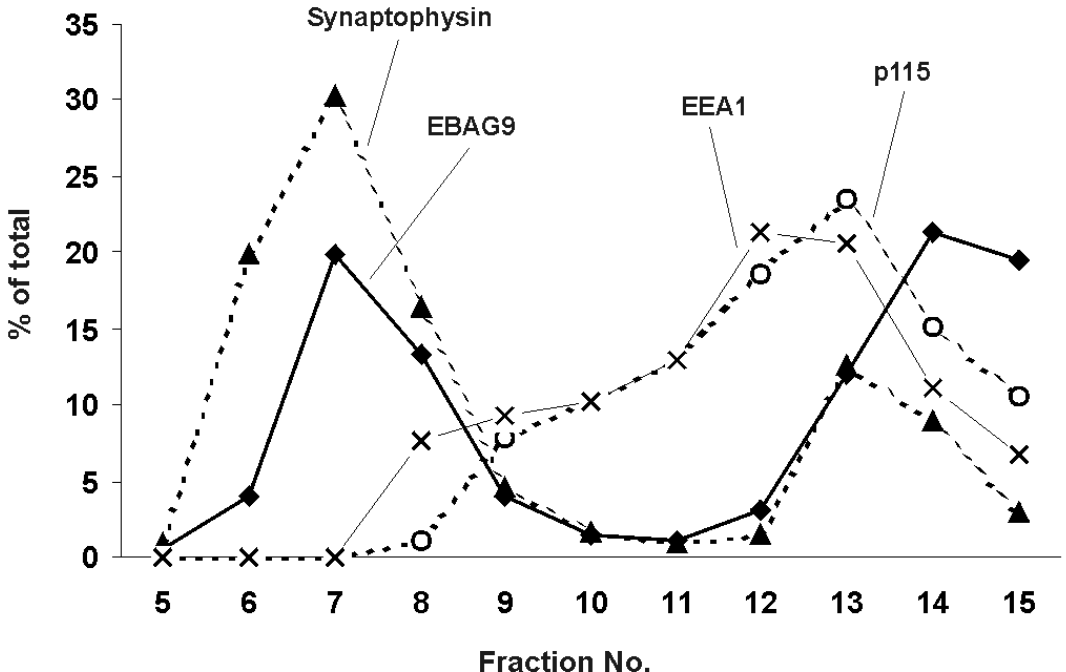
Synaptophysin
EBAG9
EEA1
p115
% of total
35
30
25
20
15
10
5
0
5 6 7 8 9 10 11 12 13 14 15
Fraction No.

Figure 8

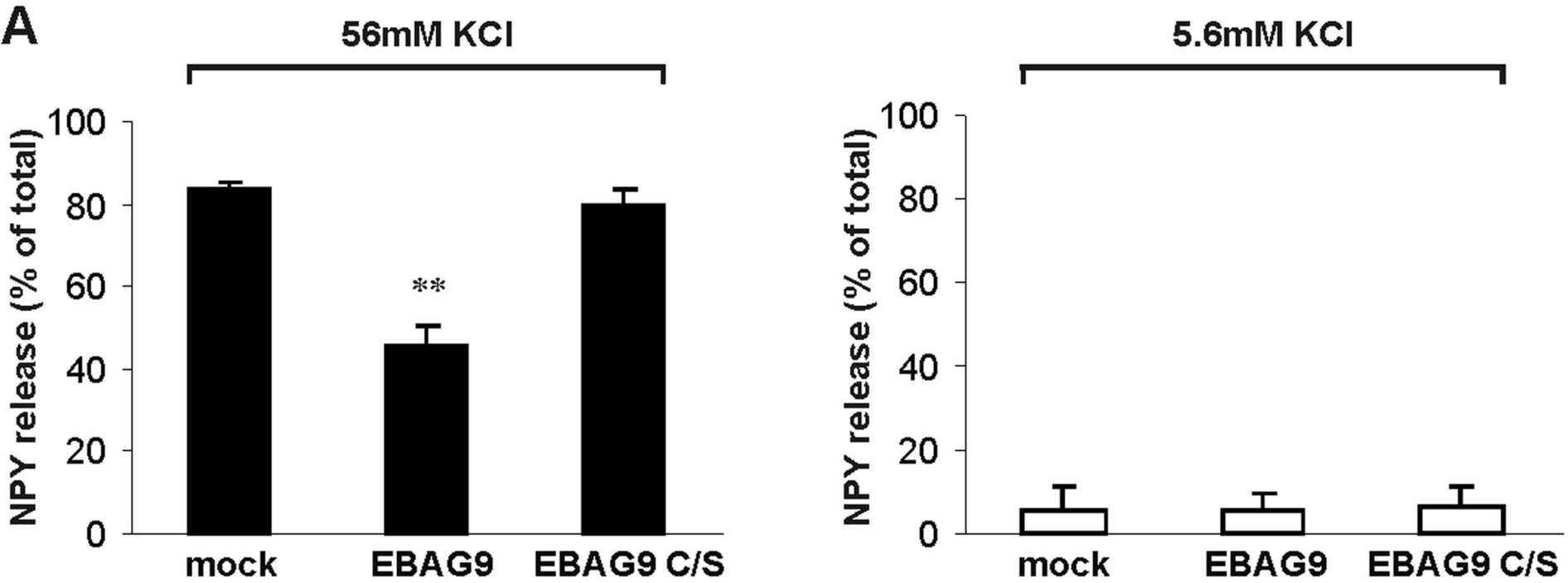
A
56mM KCl
5.6mM KCl
NPY release (% of total)
100
80
60
40
20
0
**
mock
EBAG9
EBAG9 C/S

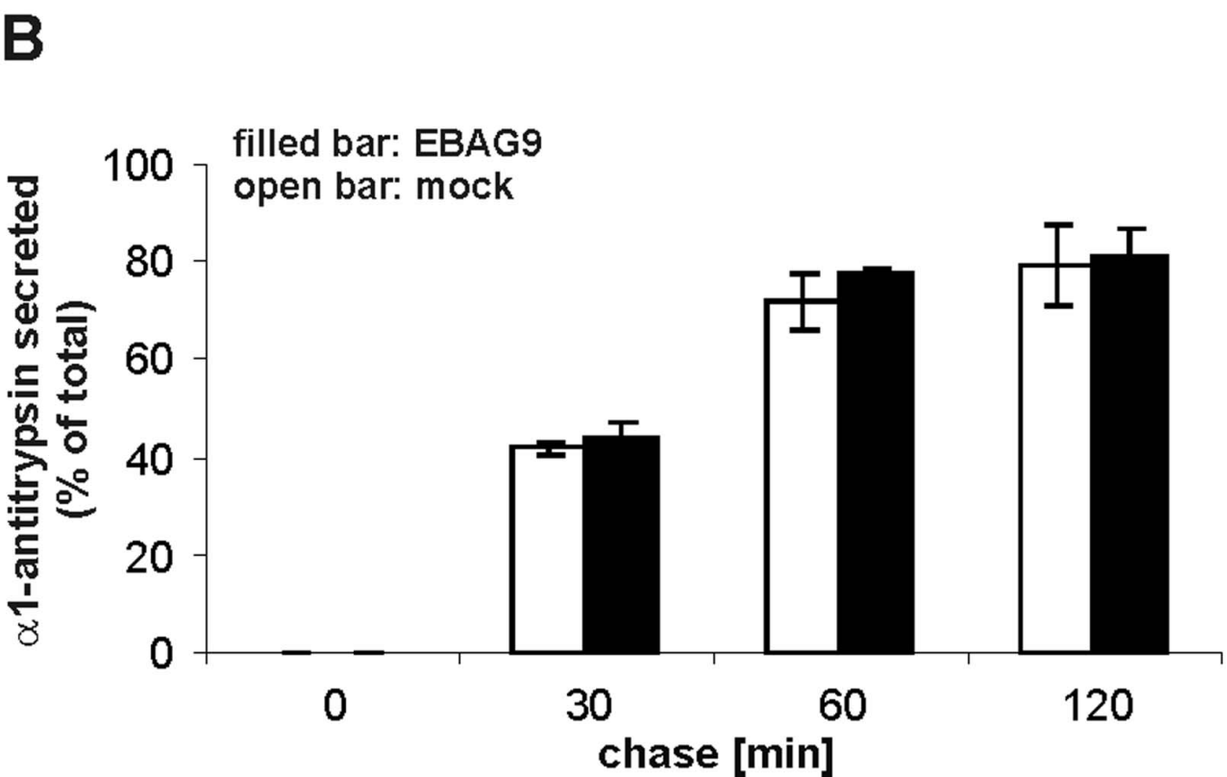
B
filled bar: EBAG9
open bar: mock
α1-antitrypsin secreted (% of total)
100
80
60
40
20
0
0
30
60
120
chase [min]

Figure 9

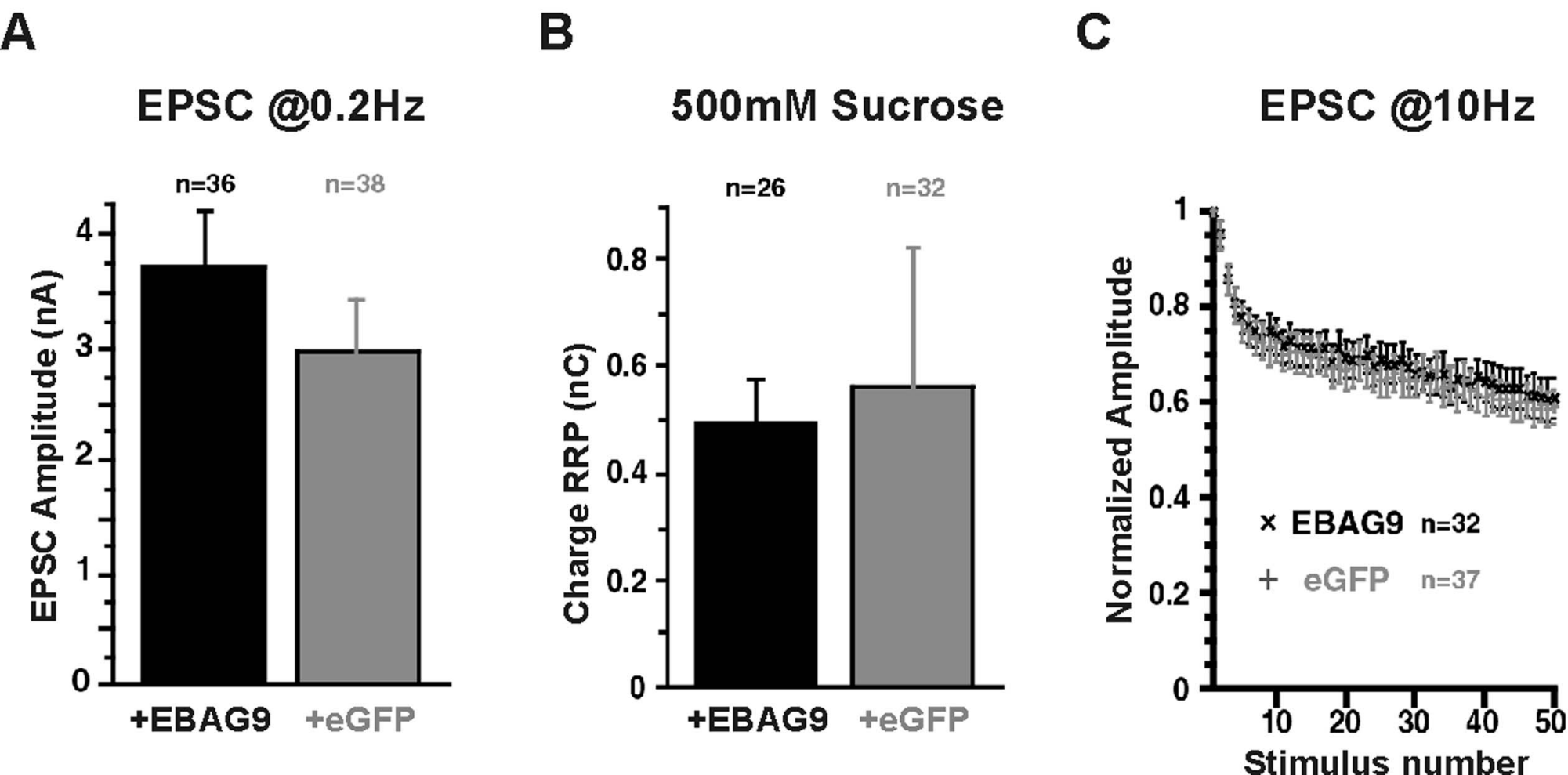
A
EPSC @0.2Hz
n=36
n=38
EPSC Amplitude (nA)
0
1
2
3
4
+EBAG9
+eGFP
B
500mM Sucrose
n=26
n=32
Charge RRP (nC)
0
0.2
0.4
0.6
0.8
+EBAG9
+eGFP
C
EPSC @10Hz
Normalized Amplitude
0
0.2
0.4
0.6
0.8
1
× EBAG9 n=32
+ eGFP n=37
10
20
30
40
50
Stimulus number

Figure 10

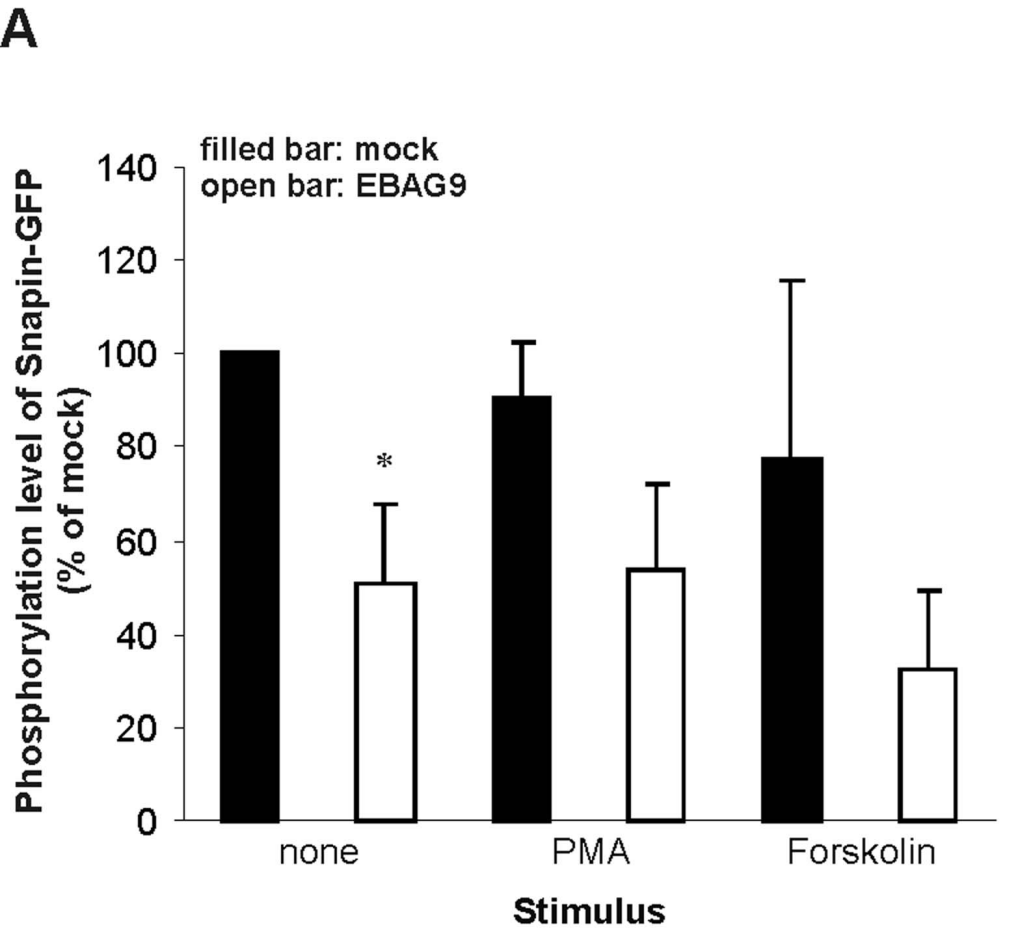
A
filled bar: mock
open bar: EBAG9
Phosphorylation level of Snapin-GFP (% of mock)
140
120
100
80
60
40
20
0
*
none
PMA
Forskolin
Stimulus

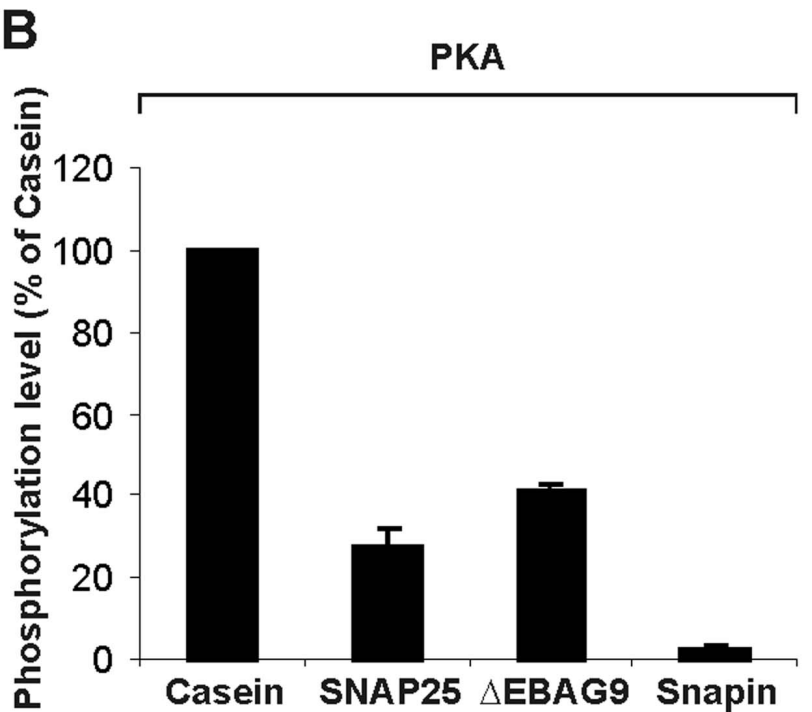
B
PKA
Phosphorylation level (% of Casein)
120
100
80
60
40
20
0
Casein
SNAP25
ΔEBAG9
Snapin

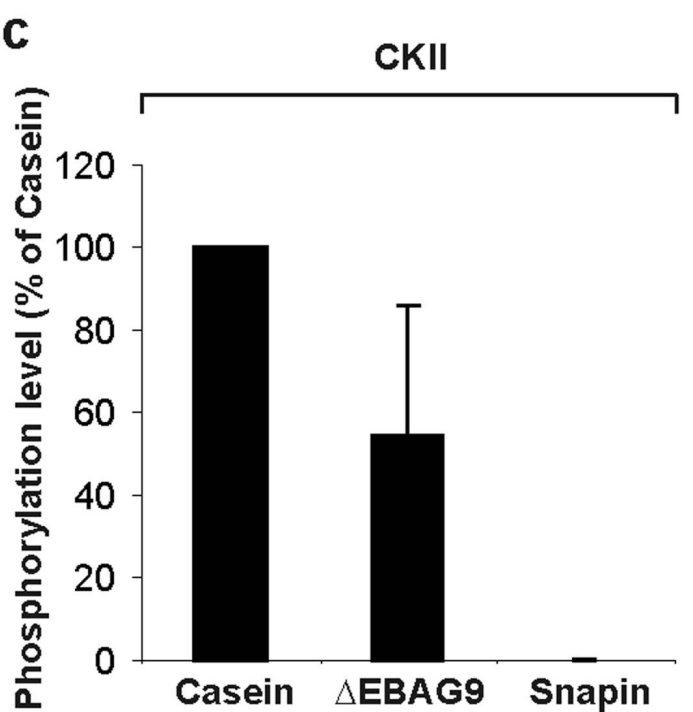
C
CKII
Phosphorylation level (% of Casein)
120
100
80
60
40
20
0
Casein
ΔEBAG9
Snapin

Figure 11

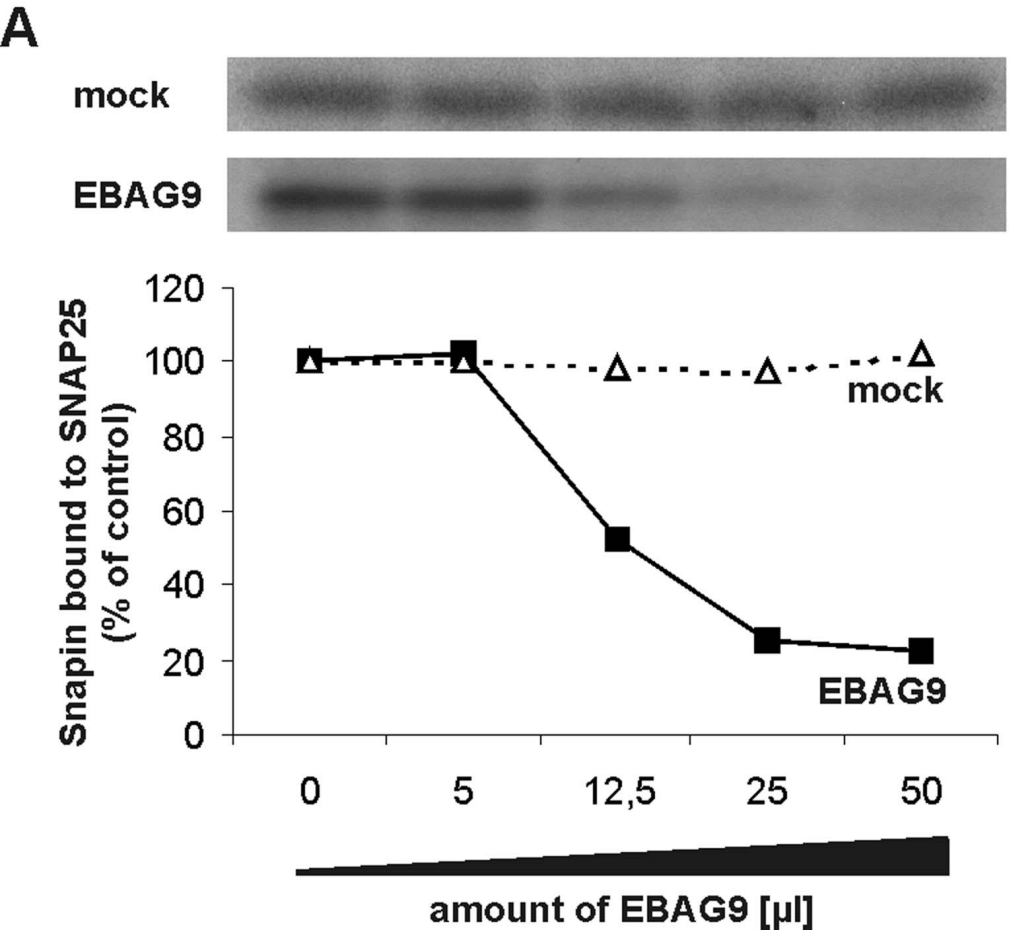
A
mock
EBAG9
Snapin bound to SNAP25
(% of control)
120
100
80
60
40
20
0
mock
EBAG9
0
5
12,5
25
50
amount of EBAG9 [µl]

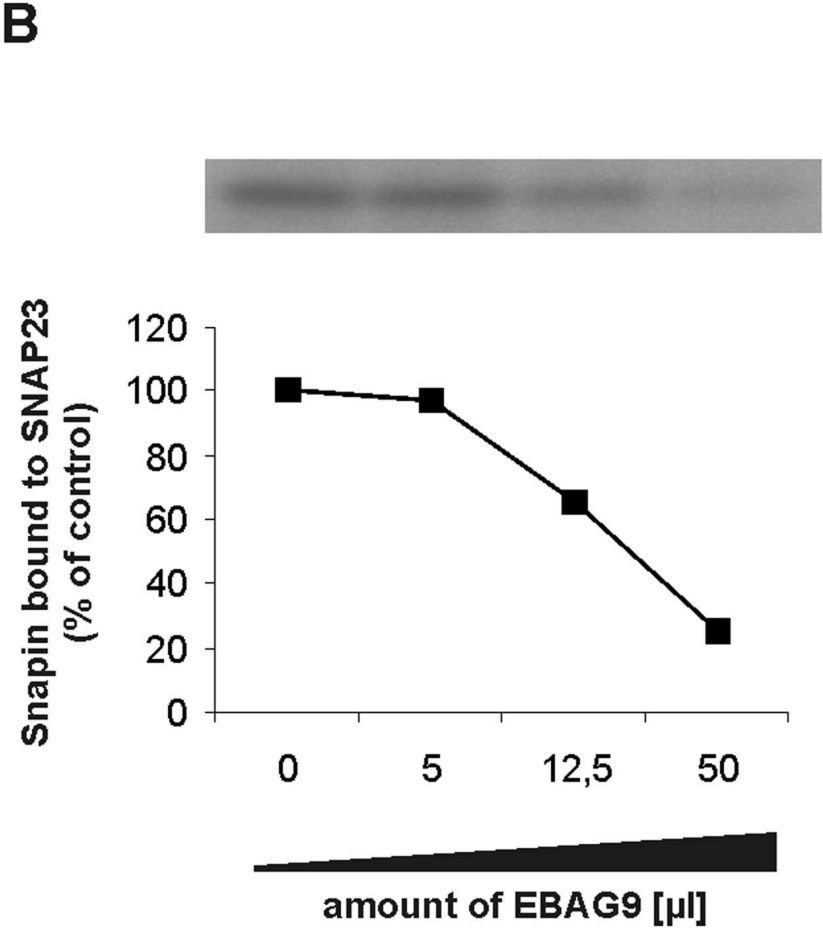
B
Snapin bound to SNAP23
(% of control)
120
100
80
60
40
20
0
0
5
12,5
50
amount of EBAG9 [µl]